2017-04-01

Ash aggregation during the 11 February 2010 partial dome collapse of the Soufriere Hills Volcano, Montserrat

Burns, FA

10.1016/j.jvolgeores.2017.01.024
Journal of Volcanology and Geothermal Research
Elsevier BV

Ash aggregation during the 11 February 2010 partial dome collapse of the Soufrière Hills Volcano, Montserrat

F.A. Burns[1], C. Bonadonna[1], L. Pioli[1], P.D. Cole[2], A. Stinton[3]

[1], Department of Earth Sciences, University of Geneva, Switzerland

[2], School of Geography Earth and Environmental Sciences, University of Plymouth, UK

[3], Montserrat Volcano Observatory, Montserrat, West Indies

Abstract

On 11 February 2010, Soufrière Hills volcano, Montserrat, underwent a partial dome collapse (~50 x 10^6 m^3) and a short-lived Vulcanian explosion towards the end. Three main pyroclastic units were identified N and NE of the volcano: dome-collapse pyroclastic density current (PDC) deposits, fountain-collapse PDC deposits formed by the Vulcanian explosion, and a tephra deposit associated with elutriation from the dome-collapse and fountain-collapse PDCs (i.e. co-PDC fallout deposit). The fallout associated with the Vulcanian explosion was mostly dispersed E and SE by high altitude winds.

All units N and NE of the volcano contain variable amounts and types of particle aggregates, although the co-PDC fallout deposit is associated with the largest abundance (i.e. up to 24 wt%). The size of aggregates found in the co-PDC fallout deposit increases with distance from the volcano and proximity to the sea, reaching a maximum diameter of 12 mm ~500m from the coast. The internal grain size of all aggregates have nearly identical distributions (with Mdϕ ≈ 4-5), with particles in the size categories >3phi (i.e. <250μm) being distributed in similar proportions within the aggregates but in different proportions within distinct internal layers. In fact, most aggregates are characterized by a coarse grained central core occupying the main part of the aggregate, coated by a thin layer of finer ash (single-layer aggregates), while others have one or two additional layers accreted over the core (multiple-layer aggregates). Calculated aggregate porosity and settling velocity vary between 0.3-0.5 and 11-21 m/s, respectively. The aggregate size shows a clear correlation with both the core size and the size of the largest particles found in the core. The large abundance of aggregates in the co-PDC fallout deposits suggests that the buoyant plumes elutriated above PDCs represent an optimal environment for the formation (particle collision) and development (aggregate layering) of particle aggregates. However, specific conditions are required, including i) a large availability of water (in this

32 case provided by the steam plumes associated with the entrance of PDCs into the ocean), ii)
33 presence of plume regions with different grain-size features (i.e. both median size and sorting) that
34 allows for the developments of multiple layers, iii) strong turbulence that permits both particle
35 collision and the transition of the aggregates through different plume regions, iv) presence of hot 36
regions (e.g. PDCs) that promote aggregate preservation (in this case also facilitated by the presence
37 of sea salt).
38
39 Key words: Accretionary Lapilli; Tephra deposits; Pyroclastic Density Currents; Particle Aggregation

1. INTRODUCTION

During an explosive volcanic eruption large amounts of fine ash (particles with diameters < 63 μm) are generated and injected into the atmosphere by buoyant plumes (e.g. Durant et al. 2009, Durant 2015), which can either generate from a central eruptive vent or eruptive fissure or can be elutriated from pyroclastic density currents (PDCs). Particle aggregation can significantly affect depositional patterns of fine ash generating secondary maxima of accumulation, increasing deposition rate and altering tephra-deposit thinning with distance from vent (e.g. Brazier et al. 1982; Brazier et al. 1983; Carey and Sigurdsson 1982; Brown et al. 2012). A better understanding of the parameters controlling and enhancing particle aggregation is fundamental to improve our understanding of tephra sedimentation and, consequently, provide a more accurate analysis of the associated hazards.

The time scale of aggregation is short (few to tens of minutes) and particles mainly collide and cluster because of complex interactions of surface liquid layers, electrostatic forces, turbulence and/or differences in settling velocities (e.g. Brown et al. 2012). Depending on the water content, particle aggregation results in the formation of *particle clusters* (including *ash clusters* (PC1), *coated particles* (PC2) and *cored clusters* (PC3)) and *accretionary pellets* (including *poorly structured pellets* (AP1), *pellets with concentric structures* (AP2) and *liquid pellets* (AP3)) (Bagheri et al. (2016), Brown et al. (2012), Sparks et al. (1997) and references therein). Water in volcanic clouds mainly originates from volatiles in the pre-eruptive magma, entrainment of moist lower tropospheric air and through the interaction with external water (e.g. ocean, lake, ground water). Due to various degrees of cementation, pellets with concentric structures, AP2 (i.e., often defined as accretionary lapilli) are more likely to be preserved in pyroclastic deposits than particle clusters and, therefore, have been described in more detail (e.g. Sparks et al. 1997). Their size ranges between 2 and 15mm (rarely reaching diameters >30mm), whereas poorly structured pellets (AP1) have been observed in the range of 100 μm up to a few mm, and ash clusters (PC1) from a few 10s μm up to ~10 cm (Brown et al. 2012). Aggregate size and typology might vary with distance from vent in a non-systematic manner, indicating a complex interaction between the spatiotemporally variable sources of liquid water and ice and the changes in eruptive styles. However, the mode of aggregating particles is typically around 5phi, i.e. 32 μm (Bonadonna et al. 2002; Brown et al. 2012; Durant et al. 2009; Rose and Durant 2011). Experimental studies suggest that both dry and wet aggregation can occur during the same volcanic event with electrostatic ash aggregates forming extremely rapidly and, in presence of water, accretionary pellets more efficiently scavenging large particles (up to a few hundred microns) due to the associated stronger binding forces (James et al. 2003; Van Eaton et al. 2012). Costa et al. (2010) also demonstrated how wet aggregation strongly depends on the ratio between the residence time of aggregating particles within the cloud region where liquid water exists and the time required for aggregates to

form. As a result, aggregation processes within the plume are likely to be more effective in moderate explosions and small plumes than in vigorous Plinian and subPlinian eruptions characterized by high ascending velocities (Costa et al. 2010).

Previous studies have shown how the formation of AP2s (i.e. accretionary lapilli) is more likely associated with the emplacement of PDCs, with only the ultra-fine (<10μm) outer layers being formed within co-PDC plumes (e.g. Brown et al. 2010, Van Eaton et al. 2013). In addition, the AP2s observed in large ignimbrites are typically associated with a large variety of morphologies and structures. As an example, Brown et al. (2010) report mostly sub-spherical accretionary lapilli with typical diameters between 4 and 12 mm (but as much as 25 mm) in the ignimbrites of the Bandas del Sur Group (Tenerife) associated with caldera-forming eruptions with volumes of 5-100 km^3. These accretionary lapilli exhibit two or more laminations of fine to very fine ash, which are typically normally graded, and surround an unstructured core of ash or a central angular pumice or lithic clast core (Brown et al. 2010). Accretionary lapilli were only found in the ignimbrite facies (abundance from <1 to 40vol%), which were commonly coupled with ash pellets <7mm sedimented at the base of the overlying co-PDC fallout deposits. However, they are typically absent from the lowermost parts of the ignimbrites. Ash pellets are different from accretionary lapilli in the terminology of Brown et al. (2010) as they are sub-spherical to ellipsoidal ash aggregates with no internal structure characterized by evidence of plastic deformation on deposition. In the phreatomagmatic deposits of the 25.4 ka Oruanui supereruption from Taupo volcano (New Zealand; about 750 km^3 of total erupted mass), Van Eaton and Wilson (2013) observed 6 types of ash aggregates, including spherical to subspherical *layered accretionary lapilli* with diameter between 5-20 mm and characterized by up to 5 concentric layers of similar sized or slightly finer ash. They also described *ultrafine rim-type accretionary lapilli* with diameters between 2 and 30 mm that have up to 3 concentric layers with one of them having high proportions of <10μm ash. Van Eaton and Wilson (2013) also observed *complexly layered accretionary lapilli* with diameters between 1 and 4 cm and composed of tens of thin outer laminations of fine to ultrafine ash. *Ultrafine rim-type* and *complexly layered accretionary lapilli* are only found in PDC deposits, while *layered accretionary lapilli* are also found in fallout deposits. Accretionary lapilli were also found in the co-PDC fallout deposit associated with the 26 December 1997 large dome collapse of Soufrière Hills Volcano, SHV (Montserrat, West Indies), even though they are associated with more homogenous morphologies across the deposit with respect to those reported by Brown et al. (2010) and Van Eaton and Wilson (2013) (Ritchie et al. 2002; Bonadonna et al. 2002), suggesting that also buoyant plumes elutriated from PDCs might favour aggregation processes.

The main objectives of this study include a systematic description of aggregate features and their spatial variation based on a detailed characterization of the pyroclastic deposits associated with the

11 February 2010 dome collapse of SHV, to understand their mechanism of formation, dispersion and sedimentation. Aggregates from both flow and fallout units were systematically sampled and characterized in order to provide new insights into the process of particle aggregation, with a specific focus on accretionary lapilli, from here on defined as pellets with concentric structures (AP2) following the nomenclature of Brown et al. (2012).

1.1 The 11 February 2010 partial dome collapse

1.1.1 Eruption chronology and dynamics

The 11 February 2010 partial dome collapse occurred at the end of Phase 5 of dome growth which was a 4 month-long period of intense extrusive and explosive activity. After 9 months of quiescence the fifth phase of lava extrusion began on 8 October 2009. Rapid extrusion, which was preceded by 3 days of ash venting, began from the summit of the pre-existing dome (Cole et al. 2014b). The activity during the following four months comprised ash venting, dome growth and piecemeal minor collapses sending block-and-ash flow (BAF) PDCs down all major drainages of the volcano. Additionally in early January and February 2010 a series of five Vulcanian explosions occurred (Cole et al. 2014a). The main growth took place on the northern flank where large blocky lobes where extruded covering the steep slopes of the 2006-2007 dome. An extensive talus deposit developed below the lobes and stretched across the northern and western flanks. The lava extrusion during this phase occurred at an average rate of 7 m^3/s (Stinton et al. 2014a). The total volume of the dome and talus before the 11 February 2010 collapse was about 248 x 10^6 m^3 (Stinton et al. 2014b).

On the 11 February 2010 at 15:52 (UTC) a northward-directed partial dome collapse occurred marking the end of the fifth Phase of extrusive and explosive activity. A volume of approximately 50 x 10^6 m^3 was removed from the dome and widespread PDCs moved down the northern flanks of SHV. The PDCs reached the sea, travelling at least 1 km offshore, and added 1 km^2 of land to the NE coast of the volcano. The collapse lasted 107 minutes with the majority of PDC activity occurring in a very intense, but brief 15-minute-long period towards the end of the event (Stinton et al. 2014b). The total activity can be summarized by six peaks in PDC generation and two Vulcanian explosions. The second, larger Vulcanian explosion was inclined 25° from the vertical in an N-NE direction (Cole et al. 2015) and generated a tephra plume that rose to about 15 km above sea level. The origin of the dome collapse was the piecemeal failure of a series of large, unstable lobes that had been recently emplaced on the northern flank of the lava dome (Stinton et al. 2014b).

1.1.2 Deposit

The 11 February 2010 partial dome collapse was marked by a complex sequence of events. Figure 1 shows the distribution of the PDC deposits on the N and NE flanks of SHV. The stratigraphy can be divided into three main units: the first was formed during the dome collapse and consists of a series of dense and dilute PDCs, the second resulted from the Vulcanian explosion that generated various pumice-flow deposits and finally the third that tops the sequence is tephra fallout associated with both elutriated plumes associated with all PDCs and the Vulcanian explosion (not shown on the map in Fig. 1).

Unit I: Dome collapse – PDC deposits

Block-and-ash flows (BAF): The bulk of the material removed during the dome collapse was emplaced as a series of BAFs that largely remained valley-confined and moved to the NE (Fig. 1). They spread out and were deposited between Spanish Point and Trant's Bay as an extensive pyroclastic fan consisting of multiple units. Each flow unit is composed of a thick heterogeneous layer (1.5 to > 3 m) containing coarse-grained, clast-supported material, which grades into coarse ash towards the top and the bottom. The blocks contained in this layer range from poorly vesiculated (density 1900-2200 kg/m^3) to dense dome rock (density >2200 kg/m^3). This layer is topped by the overlying co-PDC fallout layer up to 25 cm thick and composed of fine ash and AP2s. In addition most BAF units contain abundant gas elutriation pipes, due to the escape of gases during deposit compaction (Stinton et al. 2014b).

Pyroclastic surges: The climactic phase of the dome collapse (82 min) was associated with dilute PDCs that moved to the NNW through Streatham and to the NNE through Harris (Fig. 1). These PDCs then continued north draining into the Farm River valley and moved eastwards and then northeastwards towards Trant's (Cole et al. 2015). The deposits were emplaced by multiple PDC pulses. Each unit is fine-grained and ash-rich with thicknesses between 10 and 50 cm. Pyroclastic fragments consist of dense or poorly vesiculated dome rock and pumice clasts are either rare or absent (Stinton et al. 2014b).

Unit II: Vulcanian explosion – PDC deposits

Pumice-flow deposit: Pumice-rich PDCs moved down three of the major northern drainages of the volcano: they reached 5 km down the Belham Valley to the NW, 4 km down White's Bottom Ghaut to the NE and 7 km down Trant's Bay to the NNE (Fig. 1). The corresponding deposits were composed of narrow sinuous lobes measuring < 20 m wide, hundreds of meters long and typically < 1 m thick (Cole et al. 2015). The rounded morphology of the pumice clasts and valley-filling morphology indicates that they were emplaced by dense PDCs, identical to those formed by fountain collapsederived PDCs

associated with most Vulcanian explosions at SHV such as those in 1997 and 2008 (Cole et al. 2002, 2014a).

Pumice-boulder deposit: On the northern flank of the volcano a widespread discontinuous deposit of pumiceous boulders overlies the dome collapse PDC deposits (Fig. 1). The clasts are rounded, with typical size of >10 cm, reaching a maximum length of 120 cm. The boulders are found embedded or protruding from the upper ash-rich layer of the dome-collapse-derived PDC deposits. The pumice flows and pumice boulder deposits are both related to the collapse of the directed fountain onto the N flank of the volcano, resulting from the inclined explosion. For more detail on the origin of the pumice boulders see Cole et al. (2015).

Unit III: co-PDC fallout deposit

The sequence of PDC deposits is topped by up to 20 cm of tephra fallout derived from co-PDC plumes containing abundant accretionary lapilli, and angular pumice fragments embedded in the upper part, (Stinton et al. 2014b) (Fig. 2). However, the co-PDC fallout deposit is clearly distinct from the main part of the Vulcanian fallout deposit. In fact, the tephra plume formed by the Vulcanian explosion was inclined towards the north and rose to an altitude of 15 km. As a result, the Vulcanian lapilli and blocks (up to 15 cm diameter) were deposited to the N and NE of the volcano, while the Vulcanian ash reaching the umbrella region of the cloud was dispersed by high winds (> 5km) across the islands of Antigua (to the NE), and Guadeloupe, Dominica and St. Lucia to the SE and S. The reader is referred to Cole et al. (2015) for full details on this event.

2. METHODS

This work focuses on the study of accretionary pellets (AP2s) associated with various pyroclastic deposits generated by the 10 February 2011 dome collapse of SHV. Samples were collected from 16 different locations at different distances from the vent (Fig. 1). The four main areas sampled from most proximal to most distal with respect to the vent are: Harris (2.5 km N of the vent), Farm (4 km NNE), Spanish Point (5 km NE) and Trant's Bay (6 km NNE) (Fig. 1). At each location, the different stratigraphic units containing aggregates were sampled. The grain-size distributions of these units were determined by combining the measurements from mechanical sieving for particles ≥ 0.5 mm (<1 ϕ) and from laser diffraction for particles <0.5 mm (>1 ϕ) (i.e. using the CILAS 1180 instrument of the University of Geneva; http://www.cilas.com/). AP2s were manually separated from their respective deposits and their size and shape were measured with a calliper when still intact. They were then crushed and their grain-size distributions were measured by laser diffraction. 92 of the individual AP2s collected were set in araldite resin in order to allow sectioning and studying their internal structure. Synthetic oil was

used as a lubricant during both cutting and polishing procedures in order to preserve soluble salt crystals. A selection of 34 AP2s was examined under the Scanning Electron Microscope (SEM) to obtain more detailed information about their internal structure and to characterize their internal grain size. Some of the processed AP2s preserved a compact structure, while others underwent partial fragmentation due to the resin contraction, but the examination of their internal structure was still possible. High resolution pictures were taken at different magnifications to have full clast images (field of view of 6.55 mm), and close up of each internal layer (field of view ranging from 0.7 to 0.2 mm) and core (field of view ranging from 0.7 to 0.45 mm).

These images were then processed in Photoshop to obtain binary images. The internal grain size of the AP2s was measured using the image analysis toolbox JMicroVision (Roduit 2006; http://www.jmicrovision.com/) on the binary images. The 2D information obtained was extracted and converted into 3D particle size distributions as a function of the internal structure of the AP2s following Cheng and Lemlich (1983) and Mangan et al. (1993). The porosity of selected AP2s was derived by weighing them with high precision scales and calculating the resulting densities by dividing their weight by their respective volume calculated based on the 3 main axes. The porosity (or vesicularity) was calculated as the difference between the AP2 density when whole and the density of the DRE (dense rock equivalent) of the AP2, measured by Helium pycnometry.

2.1 Sampling of the pyroclastic deposits

The deposits associated with the 11 February 2010 partial dome collapse and explosion (BAF, surge, pumice flow and co-PDC fallout deposit) were sampled at different locations (Fig. 1) with a particular focus on the study of AP2s (see Appendix I for complete stratigraphic sections). Please refer to Stinton et al. (2014b) for a complete description of the deposits.

Harris

At Harris both the surge and the co-PDC fallout deposits are present (Fig 2 and Appendix I); however, AP2s are not present in all outcrops and all units. Sample Ha-02 was collected from the upper part of the surge deposit, where the AP2s were concentrated, while sample Ha-03 was collected near the middle of the surge deposit where the AP2s were concentrated in gas-escape pipes (sample locations are indicated as an "X" in Appendix I). Sample Ha-01 was collected from the co-PDC deposit even though AP2 were not present.

Farm

At Farm all units were present: surge, pumice flow, BAF and co-PDC fallout deposits, with the surge deposit directly overlying the 1997 deposits (Fig 2 and Appendix I). In the first outcrop (Fa-01), AP2s were present both in multiple layers within the same unit (e.g. samples FA-01A and FA-01B, top and

bottom of pumice-flow deposit, respectively) and in different units in the same outcrop (e.g. FA-01C, surge deposit). AP2s were also present both in the co-PDC fallout (Fa-03A) and surge (Fa-03B) deposits. Finally, only one sample was collected in the second (Fa-02, pumice-flow deposit) and forth (Fa-04, co-PDC fallout deposit) outcrop, as AP2s were only present at the top of the deposits.

Spanish Point

The two units present in this area are the BAF and the overlying co-PDC fallout deposit (Fig 2 and Appendix I). In the first outcrop (Sp-01), AP2s were present both in multiple layers within the same unit (e.g. samples Sp-01A and Sp-01B, top and bottom of co-PDC fallout deposit, respectively) and in different units in the same outcrop (e.g. Sp-01C, BAF deposit). AP2s were also present both in the coPDC fallout (Sp-02A) and BAF (Sp-02B) deposits. Finally, only one sample was collected in the third (Sp-03) and forth (Sp-05) outcrops, as AP2s were only present at the top of the co-PDC fallout deposit. The forth outcrop (Sp-04) is not shown in the appendix as it is very similar to Sp-05 and was not sampled for aggregates (data were only used for the isopach and isopleth maps).

Trant's

This area contained extensive BAF deposits that were topped by co-PDC fallout deposit (Fig 2 and Appendix I); however, only the co-PDC fallout deposit contained AP2s (either in one or two distinct layers at different stratigraphic height). Sample Tr-01A was collected from the first 7 cm of the coPDC fallout deposit at the first outcrop, and sample Tr-01B was taken from the underlying 12 cm of the same unit. Only one sample was taken from the co-PDC fallout deposit of the second outcrop (sample Tr-02), as only one layer of AP2s was present. Samples Tr-03A and Tr-03B were collected from the very top of the co-PDC fallout deposit of the third outcrop, while sample Tr-03C was collected from the bottom of the same unit, all of which contained AP2s. Deposits in the last outcrop were not fully exposed and, therefore, only the co-PDC fallout deposit with abundant AP2s was sampled (sample Tr-04).

3. RESULTS

3.1 Physical characterization of the co-PDC fallout deposit

3.1.1 Isopach map and volume of the co-PDC fallout deposit

The thickness of the co-PDC fallout deposit measured in various locations was combined with that of Stinton et al. (2014b) to compile a comprehensive isopach map (Fig. 2). The maximum thickness of the deposit (24 cm) was measured in the Trant's Bay, near the end of the BAF deposit. The thickness then decreases regularly away from the sea. The isopach lines are elongated ellipses orientated 30° NE and centered on the maximum thickness (24 cm) at Trant's. The integration of both the exponential and

Weibull fitting of thickness data (Pyle 1989; Bonadonna and Costa 2012) results in a bulk volume of about 2 x 10^6 m^3, with an associated mass of about 2.4 x 10^9 kg and a DRE volume of 9.2 x 10^5 m^3 (assuming a density of 1200 kg/m^3 for the co-PDC deposit and of 2600 kg/m^3 for the dense juvenile material as in Bonadonna et al. (2002) and Druitt et al. (2002)). The total volume of material removed during the 11 February 2010 dome collapse is of 50 x 10^6 m^3 (Stinton et al. 2014b), which corresponds to a DRE volume of 10^7 m^3 (considering an average dome porosity of 20%; Melnik and Sparks 2002). As a result, the co-PDC fallout deposit represents about 9% of the total collapse DRE volume, which well agrees with the 10-13% observed for the 26 December 1997 large dome collapse (i.e. 35-45 x 10^6 m^3; Bonadonna et al. 2002). Interesting to note that the small to moderate dome collapses in 1996 and 1997 and the fountain-collapses associated with the Vulcanian explosions in 1997 (<12 x 10^6 m^3) are associated with lower elutriation fractions (i.e. 4-5%; Bonadonna et al. 2002).

3.1.2 Grain size of co-PDC fallout deposit and abundance of aggregates

An example of the grain-size distribution for the co-PDC fallout deposit is represented by sample Tr02 (Fig. 3), with an Md_ϕ of 4.3. The grain-size distribution is strongly bimodal when most AP2s are left intact (e.g. Fig 3a). However, the bimodality mostly disappears when the AP2s are crushed (e.g. Fig 3b). In addition, particles in the size categories >3 phi aggregated in similar proportion (Fig. 3b), indicating a similar aggregation coefficient. As expected, sorting of co-PDC fallout mostly increases with decreasing deposit grain size (Fig. 3c). The Md_ϕ map for the co-PDC fallout deposit (Fig. 4) shows the distribution of the median grain size with all AP2s crushed. The Md_ϕ isograde can be approximated to elongated ellipses orientated 30° NE, which is the same direction as for the associated isopach map. The coarsest deposit has Md_ϕ =2.8 and was found in the location with the maximum measured thickness (Fig. 2). However, the abundance of AP2s shows only a weak correlation with deposit grain size, with both the highest and the lowest values (i.e. 24% and 3%) being associated with similar deposit Mdϕ (i.e. 4.3 and 4.1, respectively) (Fig. 4). As the distance from the maximum thickness of the deposit and the sea increases, the abundance in AP2s decreases from a maximum of 24 wt% to a minimum of 2-3 wt% inland, <500m to 2 km, respectively (Fig. 4).

3.2 Characterization of ash aggregates

3.2.1 Occurrence, morphology, porosity and terminal velocity

The abundance of AP2s within the different deposits varies significantly (Table 1): it appears low in the pumice flow deposit (extending up to 5.3 km NNE of the vent) (i.e. 2-4 wt%) and in both the surge deposit (extending up to 3.5 km North of the vent) and in the BAF deposit (extending up to 5.5 km NE of the vent) (i.e., < 8wt%), while it reaches higher values in the co-PDC fallout deposit (i.e. 224 wt%).

In addition, AP2s have been found to accumulate in distinct layers within the same outcrop (both within the same and/or in multiple stratigraphic units (Appendix I).

The sampled AP2s were classified according to their morphology. Three different types of morphologies have been determined according to the following criteria: 1) spherical AP2s, which are equidimensional (dimensions a≈b≈c); 2) oblate AP2s (dimensions a≈b>>c); and 3) irregular-shaped AP2s (dimensions a≠b≠c). We consider that the spherical AP2s mostly maintained their original morphology and dimensions, while the oblate AP2s have been flattened and the irregular shaped AP2s represent broken parts of larger AP2s that were then coated in a finer layer of ash. Most deposits are dominated by oblate to spherical morphologies (Fig. 5a and Table 1).

Calculated density of selected AP2s in both the co-PDC fallout deposit and the pumice-flow deposit ranges between about 1300 and 1900 kg m^{-3} (average of 1550 kg m^{-3}) which, accounting for a DRE density of 2656 ± 2 kg/m^3, results in porosity between 0.3-0.5 (average of 0.4; Fig. 5b). These values are within the typical range observed for accretionary lapilli, i.e. 1200-1600 kg m^{-3} and 0.3-0.5 for density and porosity, respectively (Sparks et al. 1997). Associated settling velocities range between 11 and 18 m s^{-1} at sea level and 13 and 21 m s^{-1} at 5 km above sea level (following the drag model of Bagheri and Bonadonna (2016)). These should be considered as maximum values of velocity as clearly the aggregates went through a process of particle accretion that increased the velocity with time. However, given that aggregation times are typically fast (as short as a few seconds; e.g. Van Eaton et al. 2012; Brown et al. 2012), we suspect that these AP2s rapidly reached their maximum velocity. As a comparison, density values and settling velocity of aggregates observed during the 2010 Eyjafjallajökull eruption (Iceland) are somewhat lower (100-1000 kg/m^3 and 0.2-4 m/s, respectively) (Taddeucci et al. 2011), which are more consistent with the density of particle clusters (Bonadonna et al. 2011; Brown et al. 2012). Our values are more consistent with the study of Van Eaton et al. (2013) that found density values and settling velocities between 1500-2000 kg/m^3 and

10-17 m/s, respectively, for the wet aggregates associated with the phreatomagmatic phases of the 25.4 ka Oruanui supereruption from Taupo volcano, New Zealand. It is important to notice that the sedimentation of AP2s in an ash-rich environment (i.e. turbulent plume) instead of free atmosphere only marginally affects settling velocity. In fact, the increase of fluid density (and also possible increase in the fluid viscosity) is associated with a decrease of settling velocity <20%.

3.2.2 Internal structure of aggregates

Two different types of internal structure were observed with the SEM:

Single-layer structure: The first basic structure consists of a thin homogeneous layer of fine ash (L1) covering a coarser inner core, with a heterogeneous distribution of particles (Fig. 6a). This structure will be referred to as the single-layer AP2.

Multiple-layer structure: The second type of structure is a multiple-layer AP2 (Fig. 6b), where the core is surrounded by two or sometimes three concentric layers of particles with variable size (L1, L2, and L3). The grain size of the core is poorly sorted and coarser than the contiguous layers; the first layer, L1, has a finer and more homogeneous grain size; the second layer, L2, has a coarse and poorly sorted grain size, similar to that of the core; the last layer, L3, is very thin and has a fine and homogeneous grain size similar to L1 (grain size is discussed in detail in the next section).

For each analysed image of an AP2 the number of layers was noted and the diameter of the AP2 and the thickness of the individual layers were measured. Fig. 7 gives an indication of the most common structure of AP2 found in different deposits and the relation between the size of the aggregate and the number of layers. Single-layer AP2s are significantly more common (75%) than the multiple-layer AP2s (25%), which equally split into 2- and 3-layer AP2s. The multiple-layer AP2s occurred only in the co-PDC fallout deposit and in the pumice flow deposit, alongside single-layer AP2s (Fig 7). The surge and BAF deposits contain only single-layer AP2s.

The size of sampled AP2s varies from just under 4 mm to 11 mm and mostly depends on the size of the AP2 core (Fig. 8a). In addition, a positive correlation exists between the equivalent diameter of the largest particles randomly distributed in the core (<700 μm; e.g. Fig. II.1 of Appendix II) and the aggregate size (Fig. 8b). This could indicate that large particles are better at scavenging ash particles from the volcanic plume and can generate large aggregates.

3.2.3 Texture and grain size of aggregates

SEM backscattered analysis of cross section of the AP2s revealed that the aggregates are composed of angular vesicular and non-vesicular ash fragments as well as free crystals (Fig. 9a). Blocky dense juvenile fragments typically compose most of the aggregates, while cuspate and pumice shards are particularly abundant in the AP2s found in the co-PDC fallout deposits. Rare Foraminifera and Radiolarians are enclosed in aggregate cores of co-PDC fallout deposit (Fig. 9b). Internal porosity is mostly limited to the space between grains; in some AP2s spherical to irregular micrometric voids are also observed (<100μm) (Fig. II.1e in Appendix II). Aggregate particles are immersed in a matrix that can be either observed as <5μm cubic, elongated or fibrous crystals or/and an amorphous substance (Fig. 9c). Due to the small size and rapid vaporisation of the crystals under an energy beam, no quantitative chemical analysis was possible; however, peaks of S, Cl and minor amounts of Na, Fe, Si and Al were noted during EDS analysis suggesting that the crystals mostly consists of Cl and S salts. Salts can be both of volcanic and/or sea-water origin. Most of the AP2s show homogeneous textures within the core and within each layer, but in some cases cores contain mm-size patches either composed of coarser or finer particles. Aggregate layers are mostly regular and related to sharp

variations in granulometry (e.g. Fig. 9d); however, sometimes they show local irregularities, and are locally discontinuous and partially merge into each other suggesting partial erosion followed by further aggregation.

The internal grain size of the AP2s was measured by crushing and analysing the particles with the CILAS. Figure 10a represents the superposition of a selection of the most representative internal grain size distributions measured for the analysed AP2s. The resulting grain-size distributions overlap and the Md_ϕ for most samples is comprised in between 4.2 and 4.7, except for the AP2s sampled from the surge deposit which have an $Md_\phi \approx 5$ (slightly finer grain size). For most of the samples' grain size distributions there is a secondary mode around $\phi=1$ which corresponds to the largest particles found in the core of the aggregates (e.g. Fig. 8b), then a main mode around $\phi=4$-5 followed by a fine tail > ϕ = 6. It is interesting to note that independently of the deposit, the aggregate internal grain-size distribution is either identical or very similar. In addition, there is a clear relation between Md_ϕ and sorting, with high Mdϕ values being associated with high sorting (Fig. 10b).

The internal grain size of a selection of AP2s was examined in further detail based on SEM images of sections. As an example, Fig. 11 shows the results for two AP2s collected at Spanish Point location. It is interesting to note that the core contains the largest grain-size variability and also contains particles with $\phi \leq 3$ (i.e. >125 μm), which are typically not contained within the external layers. In addition, layers 1 and 3 have a similar grain size distribution with particles ≥ 5 ϕ (i.e. ≤63 μm), while layer 2 contains particles ≥ 4 ϕ (i.e. ≤125 μm). Md_ϕ values were also calculated for each individual layer of both single-layer and multiple-layer AP2s not taking into account the largest particles observed in the core (Fig. 8) in order to allow for a better inter-comparison (Fig. 12). In single-layer AP2s cores occupy from 65 to 90 vol % and are coarser grained (Md_ϕ ranges from 4.9 to 5.5) than the external layer, whose Md_ϕ ranges from 6.3 to 7.6. An alternation of fine and coarse layers marks multiple-layer AP2s. The cores, which occupy 15 to 70 vol% of the AP2, appear to be coarser grained with an Md_ϕ ranging from 4.6 to 5.5, whereas the adjacent layer (L1) is always finer with Md_ϕ ranging from 5.6 to 7.5. Layer 2 is coarser (Md_ϕ from 5 to 5.7). Finally, the layer 3 is fine grained, with Md_ϕ ranging from 6.6 to 7. The volume occupied by single layers ranges from 5 to 70 %, with the largest values represented by (the coarse) layer 2. The Md_ϕ values measured for the cores all have values close to 5 (from 4.7 to 5.6) as in the single-layer AP2s, suggesting that the cores are of same origin and formation process and contain particles of identical grain sizes. The core and layer 2 have similar grain sizes, with the core being only slightly coarser.

3.2.4 Isopleth map of aggregates associated with the co-PDC fallout deposit

The isopleth map (Fig. 13) shows the spatial distribution of the largest AP2s collected from the coPDC fallout deposit. The values shown on the map are the average value of the three axes of the five largest AP2s sampled at each location. The maximum AP2 diameters (12 to 10 mm) are located in Trant's Bay which coincides with the maximum thickness of the co-PDC fallout deposit on the isopach map (Fig 2). The diameter of the largest AP2 gradually decreases with distance from the central maximum in Trant's to become 7 mm in Spanish point and Farm.

4. DISCUSSION

4.1 Occurrence, abundance and grain size of aggregates in the different deposits

AP2 aggregates were found in all pyroclastic deposits associated with the 11 February 2010 dome collapse of SHV (i.e. both co-PDC and PDC deposits), but associated with different facies and abundances (see also stratigraphic columns shown in Appendix I). In particular, AP2s found in PDCs are mostly concentrated in layers a few centimetres thick located at various stratigraphic heights and containing nearly exclusively aggregates; some AP2s are also found in escape pipes. AP2s found in coPDC fallout deposits can also be either matrix-supported or clast-supported mixed with coarse ash. AP2s were mostly found in association with the co-PDC fallout deposits (up to 24 wt%) and were significantly less abundant in the PDC deposits, i.e. <8 wt% (Table 1). It is important to bear in mind that some AP2s might have been broken at the impact with PDCs and, therefore, these percentages can only be considered as indicative.

Most AP2s are found NE of Harris location with a maximum abundance close to the sea. The diameter of AP2s varies between 12 mm (in the co-PDC fallout deposit sampled in Trant's) and 1 mm (in the surge deposit at Harris) (Fig. 13). The largest AP2s sampled from the surge deposit in Harris are 11 mm in diameter. The largest AP2s found in the pumice flow and the underlying surge deposits sampled in Farms are 9 and 6 mm in diameter, respectively. It is interesting to notice that in Farms, the pumice flow is characterized by two distinct layers of AP2s (located at 5-10 cm and 45-50 cm from the top, respectively; Appendix I), with the uppermost layer being rich in multiple-layer AP2s (mean diameter of ~9 mm and abundance of 4.2wt%) and the lowermost layer being rich in singlelayer AP2s (mean diameter of ~8 mm and abundance of 1.9wt%). The largest AP2s sampled from the co-PDC and underlying parent BAF deposit in Spanish Point are 9 and 8 mm in diameter, respectively. Both the co-PDC fallout deposit sampled at Trants and at Spanish Point show two distinct layers of AP2s, which represent a mixture of multiple- and single-layer AP2s (Appendix I). The occurrence of AP2-rich layers within the same stratigraphic unit and/or different stratigraphic unit of the same outcrop (e.g. pumice

flow and surge deposits at Farms and co-PDC fallout deposits at Trant's and Spanish Point; Fig. 14c and Appendix I) indicates multiple events of discrete AP2 sedimentation.

While AP2 abundance varies for different deposits, most of them having sedimented in co-PDC fallout deposits, the grain size does not show significant variations. In particular, the most represented size classes of AP2s are between ϕ=-2 and ϕ=0, corresponding to diameters between 8 and 1 mm, irrespective of deposit type (e.g. Fig. 3). As also suggested by Van Eaton et al. (2013), this type of observations may be slightly biased towards the coarsest sizes since, when manually separating the AP2s from the rest of the deposit, the largest AP2s can be more easily handled. Therefore, there may very well be a larger population of AP2s < 2 mm that was not taken into account because of the difficulty in visual detection

4.2 Abundance and grain size of the aggregates in the co-PDC fallout deposit

The isopach and Mdϕ maps of the co-PDC fallout deposit and the isopleth map of the AP2s found in the co-PDC fallout deposit show a similar trend with the maximum thickness and grain size being centred about 1 km inland from the coast along the BAF deposit (Figs 2, 4 and 13). The maximum aggregate diameters (12 to 10 mm) are found at Trant's, which coincide with the maximum measured thicknesses of the co-PDC fallout deposit (24 to 21 cm) (Figs 2 and 13). This maximum shift with respect to the central vent location confirms that the source of the fallout deposit is indeed the co-PDC plumes and not the vent plume (which was blown SE). The most intense co-PDC plumes must, therefore, have formed close to the coast. The largest AP2s (Fig. 13) were also found associated with the coarsest co-PDC fallout deposit (Fig. 4) either because they settled together with aerodynamically equivalent particles (i.e. coarse ash and lapilli) or because their cores consisted of large particles. Based on the detailed grain-size analyses (e.g. Fig. 3) we conclude that the particles contained in the cores of AP2s are not abundant enough to shift the whole deposit grain-size distribution. As a result, we consider that the largest aggregates sedimented together with aerodynamically equivalent particles (i.e. coarse ash and lapilli). Nonetheless, the relative abundance of AP2s is only weekly correlated with deposit grain size (Figs 5 and 4). In fact, it seems that the controlling factor of AP2 abundance in the co-PDC fallout deposit is the distance from the coast (Fig. 4). This confirms that proximity of the sea is an important factor since vapour concentration is one of the main parameters that enhance the aggregation process (e.g. Mayberry et al. 2002).

A few studies examining how the aggregates vary in size with distance from the volcano within a fallout deposit have been carried out. Most of them have shown that accretionary lapilli decrease in diameter with distance from the source (e.g. accretionary lapilli in phreatoplinian fallout deposits, New Zealand, decrease in diameter from 20 to 5 mm over a distance of 50 km (Self 1983)). In contrast aggregates present in the ash fall deposit of the 1980 Mount St. Helens eruption increased in size away

from the volcano (Sisson 1995). Ritchie et al. (2002) demonstrated that the aggregates within the co-PDC ash layer associated with the 26 December 1997 dome collapse of SHV also increase in size away from the volcano. In conclusion, there seems to be a general tendency for the AP2s present in fallout deposit to decrease in diameter with distance from the source, but it is not systematic, since the size of the AP2s depends on both the size of the plume and the level of moisture present in the cloud (of both volcanic and external origin, e.g. atmosphere, sea, lake, ground water).

4.3 Morphology, structure and internal grainsize of the aggregates

The majority of the AP2s analysed in this study have an oblate ($a \approx b >> c$) or spherical ($a \approx b \approx c$) morphology, while the rest have an irregular morphology ($a \neq b \neq c$) (Fig. 5a and Table 1). The irregularity and elongation of the AP2s can be due to differences either in their mechanisms of formation, or to sedimentation processes. As an example, if an irregular particle is lightly coated by fine ash, the final aggregate might keep the original shape of the core particle. On the other hand, aggregates might be elongated by compaction due to static pressure after embedding into the deposit. Aggregates might also be elongated when formed within PDCs (e.g. cylindrical aggregates in Scolamacchia et al. 2005). However, the majority of AP2s sampled from the co-PDC fallout deposit have an oblate shape and concentric layers that modified the original shape of core particles, suggesting that the elongation is either due to compaction post-deposition or to impact during deposition and transport. The AP2s that settle inside a PDC will likewise suffer from loading and may also collide with lapilli and large particles, resulting in a larger proportion of irregular and broken AP2s. Brown et al. (2010) have previously described the erosion of aggregates in PDCs due to collision and friction resulting in breakage and/or discontinuation of accreted layers. In all cases, the aggregates which have retained their spherical shape are only a minority. However, we note that for the eruption studied here, irregular AP2s showing internal erosional features were also found in the co-PDC fallout deposit (Fig. II.1f; Appendix II).

The two main types of internal structures defined for the aggregates are the single-layer AP2 and the multiple-layer AP2. The two types of structures have a central core that constitutes the main part of the aggregate (60 to 90%vol). The internal layers are distinguishable because they have different grain sizes (as described earlier in section 3.2.2).

The final size of the aggregates is not determined by the number of layers accreted (Fig. 7), but more likely by the size of the AP2 core and of the largest particle observed in the core (Fig. 8). In fact, a linear trend shows that as the diameter of the core increases (and of the largest particles observed in the core) so the diameter of the aggregate increases (Fig. 8). This also suggests that the core forming phase is the most important phase of the aggregates' history and that the accreted layers have a lesser relevance in their final dimension. There must be a critical size for the aggregate beyond which its terminal fall velocity becomes too high, and it can no longer be sustained by the buoyant forces and

513 will settle from the turbulent current. Based on our observations, the critical aggregate size for the 11
514 February 2010 co-PDC plumes is about 11-12 mm. This implies maximum core sizes of about 10-11
515 mm, allowing 1 mm for layer 1, if it is a single-layer AP2. The critical aggregate size will vary according
516 to the buoyancy and the structure of the plume, with the edges of the plumes being characterized by
517 lower upward velocity. Our calculations show that the observed AP2s had settling velocities ranging
518 between 11 and 21 m s^{-1}, so, in order to settle, they must have encountered plume regions with lower
519 velocities.

520 Regardless of the different dome-collapse dynamics, the co-PDC fallout deposit of the 11 February
521 2010 collapse shows important similarities with the 26 December 2006 collapse. In fact, the co-PDC
522 fallout deposit of the 26 December 2006 collapse (Unit III of Ritchie et al. 2002) is a 4-6 cm thick,
523 normally graded layer, composed of fine ash with abundant lenticular accretionary lapilli typically of 5
524 mm but up to 11 mm in diameter. Aggregate diameter also increased away from the volcano and
525 towards the sea (Ritchie et al. 2002) and the internal grain-size distribution had an Mdϕ value of about
526 5 (Bonadonna et al. 2002). This suggests that, regardless of the eruptive dynamics, the critical
527 aggregate diameter is around 11-12 mm and the internal grain-size distribution of aggregate is around
528 Mdϕ=5.

529 By coupling laser diffraction method and image analysis, it was possible to compare the bulk grain
530 size (based on the laser diffraction) and the internal grain size of each part of the AP2s (core and layers
531 1, 2, 3). The internal grain size distributions of the AP2s obtained with the CILAS all overlap and have
532 an Md_ϕ between 4.2 and 4.7, except for the two samples from the surge with an Md_ϕ closer to 5 (Fig.
533 10). The fact that all the grain-size distributions are so similar for all samples indicates that aggregation
534 is a markedly stable and size-selective process, selecting particles with $\phi \geq 1$ (i.e. particles with
535 diameter ≤ 1mm). This hypothesis is confirmed by the fact that in any of the analysed samples the AP2
536 Md_ϕ is about 4, whereas the Md_ϕ of the deposit varies in between 3.3 and 4.3. Therefore, the internal
537 grain size of the AP2s does not depend on the grain size of the deposit they were found in. Recent
538 studies on the particle size distribution of aggregates (Bonadonna et al. 2002; Durant et al. 2009; Brown
539 et al. 2012; Bonadonna et al. 2015; Van Eaton and Wilson 2013) have shown consistent distributions
540 for given types of aggregates: 5 phi for AP1 and AP2 aggregates and 6 phi for PC1 (ash clusters). The
541 particle size characteristics of aggregates do not therefore vary as a function of different eruptive
542 styles. This means that the identification and measurements of aggregation particle size
543 subpopulations in recent fallout deposits can be used as a tool and extended to ancient and historic
544 ash deposits.

545 The grain-size distributions inside the core and layer 2 are typically similar (e.g. Fig. 11). They are
546 both poorly sorted and contain particles <500 μm ($\phi \geq 1$) for the core (Md_ϕ varying from 4.7 to 5.6; Fig.

12) and <125 μm (ϕ ≥ 4) for layer 2 (Md_ϕ varying from 5 to 5.6; Fig. 12). These two parts of the aggregate must have been accreted in a similar environment where coarse particles are available. In contrast, layers 1 and 3 are well sorted and contain particles <63 μm (ϕ ≥ 5) for layer 1 (Md_ϕ varying from 5.8 to 7.6; Fig. 12) and <32 μm (ϕ ≥ 6) for layer 3 (Md_ϕ varying from 6.6 to 7; Fig. 12).

The thicknesses of the different layers vary in a characteristic way according to their grain size: the finer the grain size, the less voluminous the layer (Fig. 12). The core and layer 2 represent the most voluminous parts of the aggregates. Unless eroded or broken, the most external layer of an AP2 (either single or multiple layer) is always the finest layer (i.e. layer 1 in single-layer AP2s and layer 3 in multiple-layer AP2s). However, the difference in volume is not representative of the number of particles constituting each layer. As a first order approximation the number of particles constituting each layer can be assessed by dividing their volume by the volume of the median size particle; results suggest that most layers contain similar amounts of particles with respect to cores, but some of the finest layers (1 and 3) might have up to two orders of magnitude more particles than the coarse one (layer 2). Internal layers are also discontinuous, indicating a continuous aggregationdisaggregation/erosion processes occurring within the turbulent current (e.g. Fig. II.1f; Appendix II).

In fact, turbulence can either favour aggregation by enhancing particle collision, but also induce aggregate breakage due to powerful collision between already formed and fragile aggregates (e.g. Brown et al. 2010). As a result, once an aggregate has been broken (resulting in partial preservation of one or more layers) in can be recycled and accrete new layers on top of the eroded ones.

4.5 Conceptual model for particle aggregation associated with the 11 February 2010 dome collapse

The 11 February 2010 dome collapse of SHV provides important new insights into the formation of AP2s. Brown et al. (2010) and Van Eaton and Wilson (2013) have suggested that accretionary lapilli with concentric internal structures are likely associated with the emplacement of PDCs and are difficult to form in Plinian plumes. Their work is mostly based on the study of large ignimbrites and accounts for a variety of AP2s ranging from simple ash pellets with no concentric structures to layered accretionary lapilli and complexly layered accretionary lapilli characterized by several outer layers. In contrast, the AP2s sampled in the pyroclastic deposits associated with the 11 February 2010 dome collapse of SHV are significantly more homogenous in both typology and grain size compared to those studied by Brown et al. (2010) and Van Eaton and Wilson (2013). In fact, they can all be classified as the *layered accretionary lapilli* of Van Eaton and Wilson (2013), the *accretionary lapilli* of Brown et al. (2010) and the *accretionary pellets with concentric structures* (AP2) of Brown et al. (2012). Their main variation is related to the number of layers (1 to 3) and the relative abundance in the different deposits (e.g. Table 1). Based on the homogeneity of both the typology and the grain size through the different

deposits and the larger abundance in the co-PDC fallout deposits, we conclude that AP2s of the 11 February 2010 dome collapse of SHV mostly formed and sedimented from the ash-rich buoyant co-PDC plumes mostly generated from multiple PDC pulses. The timing of particle aggregation can be as short as a few seconds (e.g. Van Eaton et al. 2012; Brown et al. 2012). As a result, we suggest that first poorly structured pellets (AP1 of Brown et al. 2012) grew in short times mostly by coalescence under liquid saturated conditions in poorly sorted regions of the co-PDC plumes and acted as massive poorly sorted aggregate cores (Fig. 13a). AP1 might have then cycled multiple times through stratified regions of the cloud characterized by different grain size and humidity conditions adding additional concentric layers and forming single-layer or multiple-layer AP2s (Fig. 13b). When these AP2s have reached aerodynamic conditions that made them unstable in the buoyant plume they sedimented within the underlying PDC deposits (BAF, pumice flows or surge)
(Fig. 13b and Appendix I). In fact, even though the main source of co-PDC plumes is most likely the BAF directly associated with the dome collapse, ash particles must have elutriated also from the less voluminous pumice flows and surges associated with the Vulcanian explosion merging within the larger BAF-generated co-PDC plumes. This is confirmed by the presence of vesicular juvenile fragments within the observed aggregates (Fig. 9). As a result, AP2s were able to sediment within all
PDC deposits. The latest stage of AP2 sedimentation is within the co-PDC fallout deposits that, nonetheless, are characterized by both single-layer and multiple-layer AP2 (Fig. 13c and Appendix I). The syn-deposition of single-layer and multiple-layer AP2s in the co-PDC fallout deposit indicates that both aggregate types could have formed at the same time in different regions of the buoyant plumes. In addition, as also mentioned in section 4.1, AP2 sedimentation must have occurred as multiple discrete events recorded by the occurrence of multiple AP2-rich layers at different stratigraphic heights probably associated with multiple PDC pulses and multiple steam explosions generated by the entrance of the PDCs in the ocean (e.g. Appendix I). Finally, many single-layer and multiple-layer AP2s in both PDC and co-PDC fallout deposits show truncated layers sometimes accreted by outer layers, indicating that aggregation-disaggregation processes occurred both in the co-PDC plumes and in the PDCs due to collision and friction. Such a process has already been described both by Brown et al. (2010) and Van Eaton and Wilson (2013).

4.5.1 AP2 formation, evolution and cementation

The formation of AP2 has already been shown to require particular eruptive and atmospheric conditions (e.g. Brown et al. 2010; Brown et al. 2012; Gilbert and Lane 1994; Mueller et al. 2016; Schumacher and Schmincke 1995; Schumacher 1994; Van Eaton et al. 2012). Our study supports the notion of Brown et al. (2010) that AP2s are more likely to form in association with the emplacement of PDCs, but, as also reported by Van Eaton and Wilson (2013) and Ritchie et al. (2002), it demonstrates

that they can also directly originate by fallout from co-PDC plumes and do not need to be transported within PDCs to form multiple concentric layers. In fact, the occurrence of AP2s with well-formed concentric layers mostly requires specific conditions that can also be found in co-PDC plumes: i) availability of water (e.g. Van Eaton et al. 2012; Mueller et al. 2016; Schumacher and Schmincke 1995; Schumacher 1994); ii) presence of poorly-sorted "wet" regions in the turbulent plume/current characterized by a wide range of particle size (<350 μm) to form a stable core (e.g. Van Eaton et al. 2012; Mueller et al. 2016; Schumacher and Schmincke 1995; Schumacher 1994); iii) presence in the turbulent plume/current of well-sorted "dry" regions characterized by fine ash to form the ash-rich outer layers (e.g. Van Eaton et al. 2012; Mueller et al. 2016); iv) enough turbulence to allow transport through different regions in the plume/current. In fact, the poorly-sorted coarseash to fine-ash "wet" regions are necessary to form a stable core (AP1) through coalescence with about 15 wt% water, while well-sorted fine-ash rich suspension cannot form stable AP1 (e.g. Van Eaton et al. 2012; Mueller et al. 2016; Schumacher and Schmincke 1995; Schumacher 1994).

In contrast, the formation of concentric layers is promoted by the availability of well-sorted fine ash, pre-existing aggregates to "seed" layering and restricted availability of liquid water to suppress nucleation of new ash clusters (e.g. Van Eaton et al. 2012). In fact, fine-ash-rich concentric layers are likely to form at low liquid water content (<10wt%) where fine ash is preferentially accreted by scavenging processes while coarse ash is excluded (Van Eaton et al. 2012). At near-saturated liquid contents >10-15wt%, aggregation coefficients of all sizes approach unity, indicating a diminishingly size selective process; when content of liquid water is above 20-25wt%, no scavenging occurs and all coarse and fine ash particles are indiscriminately collected by slurried droplets (i.e. mud rain) (Van Eaton et al. 2012; Schumacher and Schmincke 1995). As a result, 14-15 wt% liquid water can be considered as a threshold for layering mechanism versus coalescence mechanism (that can form stable cores). Van Eaton et al. (2012) have shown that even at >15 wt% water, particles >200μm are rarely incorporated within the aggregates. As a result, the large particles observed in the 11 February 2010 aggregates ranging between 200 and 700 μm (Fig. 8) might represent the core "seed" on to which smaller particles have started accreting. The weak positive relationship between the largest core particles and the overall aggregate diameter indicates that larger particles might promote scavenging and aggregate growth (as the largest part of the aggregate is the actual core). As a comparison, a weak positive relationship between the core diameter and the rim volume was observed by Van Eaton and Wilson (2013) also suggesting that the larger cores are somewhat more effective at scavenging fine grained outer layers.

The formation of fine-ash-rich outer layers might be explained by electrostatic forces at low water content (e.g. Ennis et al. 1991; Van Eaton et al. 2012). An additional parameter important for the

stability of AP2s is the presence of hygroscopic species (e.g. sulphate, gypsum crystals and salt), that have often been reported as necessary to promote cohesion (e.g. Gilbert and Lane 1994; Mueller et al. 2016; Sparks et al. 1997). Our study also supports the idea that sea salt might have promoted the cohesion of the AP2 formed during the 11 February 2010 dome collapse of SHV. In fact, salt was observed in AP2s from all deposits and in all AP2 portions (i.e. cores and layers). Nonetheless, hygroscopic species are not universally required in abundance to keep aggregates together, and it may be that only small amounts of secondary precipitations might promote cementation (e.g., Van Eaton et al. 2012). Mueller et al. (2016) have also stressed that salt-driven cementing would require not only an abundance of pre-existing soluble salts, but also rapid drying after formation. In fact, their experiments show that AP2s left in humid environment more likely disaggregate than AP2s that passed through low humidity regions. Low humidity regions can be achieved in volcanic settings, e.g. sedimentation into drier atmosphere or recycling from cold regions of the plumes into hotter regions of either plumes of PDC (>100 °C) (Mueller et al. 2016). In the case of the 11 February 2010 dome collapse of SHV these temperatures can be easily reached both in the PDCs and in the overlying coPDC fallout deposits sedimenting onto hot PDCs.

4.5.2 The role of volcanogenic meteorological clouds

Volcanogenic meteorological clouds (i.e. water clouds originating from the interaction of a hot PDC with the ocean surface; Fig. 13) play a fundamental role in the formation of AP2 (e.g. Mayberry et al. 2002). The large amount of vapour released from the associated steam explosions drives buoyancy in the co-PDC plumes and provides an important source of water to form liquid and solid phases necessary for both the stabilization of the AP1 aggregates and the growth of AP2 aggregates. In fact, ice is a dominant phase at about 6 km altitude where temperature is generally colder than -40 °C (Herzog et al. 1998), and, therefore, will be a dominant phase in most plumes above 6 km.

As an example, the hot ash heating the ocean surface during the 26 December 1996 dome collapse of SHV (associated with a main co-PDC plume of about 15 km) produced a volcanogenic meteorological cloud that reached about 17 km of altitude (Mayberry et al. 2002). Given the similar volume of the 11 February 2010 dome collapse and of the elutriated mass, we expect both the coPDC plume and the volcanogenic meteorological cloud to reach altitudes greater than 6 km (assuming that the mass was elutriated at a similar rate). The volcanogenic meteorological cloud of the 26 December 1996 dome collapse contained a maximum mass of ice of 1.5×10^8 kg and dissipated after about 6 hours, possibly due to mixing and evaporation or ice hydrometeor sedimentation (Mayberry et al. 2002).

The presence of excess water/ice can scavenge SO_2 from the volcanic plumes, because SO_2 is either dissolved in the super-cooled water, or captured within or on the surfaces of ice hydrometer which

684 then sediment (Mayberry et al. 2002; Rose et al. 1995; Tabazadeh and Turco 1993; Textor et al. 2003).
685 The capture of ice crystals or excess liquid water in the initial aggregation process may also result in
686 the formation of irregular cavities of accretionary lapilli (e.g. Van Eaton et al. 2012). Some spherical
687 cavities/voids probably related to the initial aggregation processes have been observed also in the 11
688 February 2010 dome collapse (e.g. Appendix II). The core may initially form through liquidmediated
689 particle binding to form a core up to a size of ~4 mm, which is the typical size raindrops reach before
690 breakup (Houze 2014). At heights greater than 6 km, water tends to freeze and icemediated particle
691 binding allows aggregate cores to reach diameters of several cm. Some support for the liquid to solid
692 water phase transition is preserved in the cores of aggregates as spherical voids, which are analogous
693 to bubbles in hailstones (Cheng 1973; Durant et al. 2002; List et al. 1972). These may form due to the
694 release of dissolved air in the water drop at the ice-water interface, resulting from different solubility
695 of gases such as carbon dioxide in water and ice. Air bubbles were also observed to form at the moment
696 of freezing in the ice nucleation experiments performed by Durant and Shaw (2005).
697 Nonetheless, Van Eaton et al. (2012) have shown a preferential scavenging of particles < 63 microns
698 from ice clusters similar to electrostatic aggregates and a limited capacity of accumulating substantial
699 ash layers. The limited number of cavities and the typical poorly-sorted nature of the AP2 cores of the
700 aggregates associated with the 11 February 2010 dome collapse tend to limit the iceinitiated
701 aggregation as the dominant mechanism, but we cannot exclude it. In any case, it is certain that the
702 volcanogenic meteorological clouds that originated from the hot ash particles heating the ocean
703 surface played a fundamental role in the formation of both AP1 and AP2 by providing both an excess
704 of water and a source of additional turbulence.
705
706 **4.5.3 Model summary**
707 The formation of AP2s requires a wide range of particle sizes (coarse to fine ash) and a large amount
708 of water (10-20 wt%) to grow the aggregate cores (AP1). The water can have different origin. As an
709 example, it can be sourced from the steam produced by secondary explosions associated with the
710 entrance of PDC in the ocean as in Montserrat (both for the 26 December 1996 and the 11 February
711 2010 dome collapses) or be related to water-magma interaction at vent for the Oruanui eruption (Van
712 Eaton and Wilson 2013). It is important to note that despite numerous dome collapses and Vulcanian
713 explosions that have taken place in Montserrat since the beginning of the current eruption in 1996,
714 only the two large dome collapses of 26 December 1996 and the 11 February 2010 massively produced
715 large AP2s that were well preserved in the deposit. All other events, even when small dome-collapse
716 and column-collapse PDCs entered the ocean, only produced ash clusters (PC1), coated particles (PC2),
717 poorly structured pellets (AP1) and liquid pellets (AP3) (Bonadonna et al. 2002). Similar poorly-sorted
718 AP1 aggregates with diameters up to 5 mm together with PC1, PC2 and AP3 have also been observed

719 in the May-June 1991 co-PDC fallout associated with small dome collapses of Unzen volcano with
720 runout distances that did not reach the ocean (10^4-10^6 m^3 DRE; Watanabe et al. 1999). In addition, the
721 aggregate core needs to be transported through different regions in the turbulent current
722 characterized by well-sorted fine ash and low liquid water content (<10wt%) in order to accrete the
723 first outer layer and form single-layer AP2s. These newly formed AP2 aggregates need to pass again
724 through a poorly-sorted "wet" region with water content between 10-20% in order to accrete a second
725 coarser layer. The outermost layer of all AP2 observed in our study is rich in fine ash. As a result, the
726 latest stage of aggregation process must be completed in a well-sorted fine-ash-rich "dry" region of
727 the turbulent current. In fact, fine-ash-rich concentric layers cannot simply form by scavenging the fine
728 ash from poorly-sorted suspensions (Van Eaton et al. 2012). Such a transport through very different
729 regions of the co-PDC plume can only be made possible by the combination between large co-PDC
730 plumes (as those associated with large dome collapses) and the large turbulence promoted by the
731 secondary explosions associated with multiple successive entrance of PDCs into the ocean resulting in
732 upward plume velocity higher than the aggregate settling velocities (i.e. 11-21 m s^{-1} in the case of the
733 AP2 aggregates found in the co-PDC fallout deposit in this study). As a comparison, the 15-km high
734 Vulcanian explosion associated with the 11 February 2010 dome collapse of SHV was characterized by
735 a velocity between 50 and 100 m s^{-1}
736
737 within the first 5 km (Cole et al. 2015). Such turbulence might have also caused the breakage of some
738 aggregates and the truncation of some of the concentric layers. Finally, the presence of sea salt within
739 the co-PDC plumes has promoted aggregate cementation. The homogeneity of typology and size of
740 AP2s within the different deposits associated with the 11 February 2010 dome collapse of SHV is likely
741 to be related to the short runout of the PDC (< 7km) that did not allow for a long duration of transport
742 of AP2 in the passing ground-hugging currents, thus inhibiting the formation of more complex
743 aggregates, such as the complexly layered accretionary lapilli characterized by several outer layers
744 found in the Oruanui eruption described by Van Eaton and Wilson (2013). In contrast, the occurrence
745 of layered accretionary lapilli in the co-PDC fallout deposits of the 11 February 2010 dome collapse of
746 SHV (i.e. AP2) instead of more simple ash pellets found in the co-PDC fallout deposits of the Tenerife
747 ignimbrite described by Brown et al. (2010) indicates that dome collapse PDC were probably more
748 turbulent and characterized by more heterogeneous plume structures with both poorly sorted wet
749 regions and well-sorted fine-ash rich dry regions. Plume turbulence and heterogeneity might also have
750 been promoted by the coalescence of multiple buoyant plumes associated with the multiple PDC
751 pulses of the 11 February 2010 dome collapse (e.g. Stinton et al.
752 2014b).
753

5. CONCLUSIONS

The study of the occurrence and abundance of AP2s within the different deposits associated with the 11 February 2010 dome collapse, as well as the examination of the internal structure and grain size of the aggregates, has revealed important mechanisms for the formation of accretionary pellets with concentric structures, AP2s (also defined as layered accretionary lapilli by previous authors). Main conclusions include:

1. AP2s were found in the three main units of the 11 February 2010 dome collapse of Soufrière Hills volcano, Montserrat (dome-collapse PDCs - both BAF and surge deposits; fountain-collapse pumice-flow deposit; and co-PDC fallout deposit) but in notably variable proportions. AP2s are the most abundant in the co-PDC fallout deposit (up to 24 wt %). PDC units contain fewer AP2s, <8 wt%. Most AP2s are found NE of Harris village, confirming the strong relation with PDC deposits that entered the ocean.

2. The morphology of most of the sampled AP2s is oblate, with a few sub-spherical and irregular ones; the oblate and irregular shapes are likely due to the deformation of the aggregates by compaction post-sedimentation and/or by impact on deposition and transport.

3. AP2s showed both a single-layer and a multiple-layer structure, with the multiple-layer AP2s being confined to the co-PDC fallout deposit and the pumice-flow deposit.

4. The size of the AP2s sampled from the co-PDC fallout deposit increases with distance from the volcano and proximity to the sea (main source of humidity) from a maximum diameter of 7 mm inland to a maximum diameter of 12 mm about 500m from the coast.

5. The largest values for the isopach map of the co-PDC fallout deposit (thickness of 24 cm) and the isopleth map of the AP2s sampled from the co-PDC fallout deposit (12 mm diameter) coincide with the minimum value of the Md_{ϕ} map of the co-PDC fallout deposit (2.8). As a result, there is a clear correlation amongst deposit thickness, deposit grain size and AP2 size. Nevertheless, the abundance of AP2s is mostly related to the proximity to the sea (i.e. main source of humidity).

6. Grain-size distributions of individual co-PDC fallout deposits are typically unimodal when all AP2 are crushed but show a strong bimodality when AP2s are kept intact; similar proportions of particles in the size categories ≥3 phi (<250 μm) aggregate, indicating a similar aggregation coefficient.

7. The consistency of aggregate internal grain size even for AP2s of different deposits and different eruptions (i.e. Mdϕ ≈ 4-5) confirms the stability and selectiveness of the aggregation mechanism.

8. Both the core size and the size of the total aggregate increase proportionally with the size of the largest particles measured in the core of the AP2s (0.2 to 0.7 mm); this indicates that coarse-ash

786 particles are necessary to “seed” large aggregates and that the availability of fine ash is not the only
787 factor related to the formation of AP2s.

788 9. Aggregate density, porosity and terminal velocity vary between 1300 and 1900 kg/m^3 (average of
789 1550 kg/m^3), 0.3-05 (average of 0.4) and 11-21 m/s, respectively.

790 10. The homogeneity of typology (all AP2s) and size (mostly 2-8 mm in diameter but as large as 12 mm
791 in the co-PDC fallout deposits) of ash aggregates through all deposits associated with the 11
792 February 2010 dome collapse suggest that they are of similar origin. However, the higher
793 abundance of AP2s in the co-PDC fallout deposit is an indication that the lofted plumes provided
794 an optimal environment for both particle coalescence (i.e. formation of AP2 core) and particle
795 layering associated with the accreting of ash. In particular, these two very different aggregation
796 mechanisms required the transition through different regions in the plume: from a poorly-sorted
797 (where both coarse-ash and fine-ash particles are available) “wet” (10-20wt% liquid water) regions
798 that allowed both the formation of stable massive cores and the accretion of the coarsest outer
799 layers (i.e. layer 2) to well-sorted fine-ash rich “dry” (<10wt% water) regions that allowed the
800 accretion of the fine-ash rich outer layers (i.e. layers 1 and 3).

801 11. Cementation and preservation of AP2s was promoted by both the presence of sea salt associated
802 with the steam secondary explosions due to the entrance of PDCs in the ocean and the passage of
803 the aggregates from colder regions in the plume to hotter regions in either the plume or the PDC.

804 12. The homogeneity of aggregate types that contrasts the large variety of aggregates associated with
805 large ignimbrites is likely to be related to the specific conditions of these co-PDC plumes that could
806 allow the formation of AP2s and the small runout of PDC that inhibited a further evolution and
807 complexity of aggregates.

808 13. The presence of distinct AP2-rich layers at different stratigraphic heights (both within the same or
809 multiple stratigraphic units), indicates that AP2 sedimentation occurred as discrete events probably
810 associated with multiple PDC pulses and multiple steam explosions associated with the entrance of
811 PDCs in the ocean.

812 14. Our study demonstrates that co-PDC plumes can provide optimal environments for the formation
813 of accretionary pellets with concentric structures but that specific conditions are required: 1) large
814 availability of water (supplied by the steam secondary explosions), 2) heterogeneity in the plume
815 structures allowing for both poorly-sorted wet regions and well-sorted dry regions (related to the
816 merging of multiple lofted plumes atop multiple PDC pulses and multiple steam plumes associated
817 with the secondary explosions due to the multiple successive entrances of PDC in the ocean), 3)
818 strong turbulence that permits both particle collision and the transition through different regions

in the plumes (related both to the multiple co-PDC plumes and multiple steam plumes being generated at different times in association with multiple PDC pulses and multiple steam explosions in the ocean), and 4) presence of hot regions that allowed aggregation cementation (related to the emplacement of PDCs), here further promoted by the presence of sea salt.

Acknowledgments. This project would not have been possible without the help of the staff of the Montserrat Volcano Observatory. We are also grateful to Mohsen Bagheri and Adam Durant for constructive discussion and to Jean-Marie Boccard for the thorough sample preparation. The study was carried out within the frame of the joint Geneva and Lausanne Master program (ELSTE) and was partially supported by the Swiss National Science Foundation (project number 200021_156255). Ulrich Kueppers and an anonymous reviewer are thanked for their constructive comments that helped improve the manuscript.

Appendix I

STRATIGRAPHIC SECTIONS

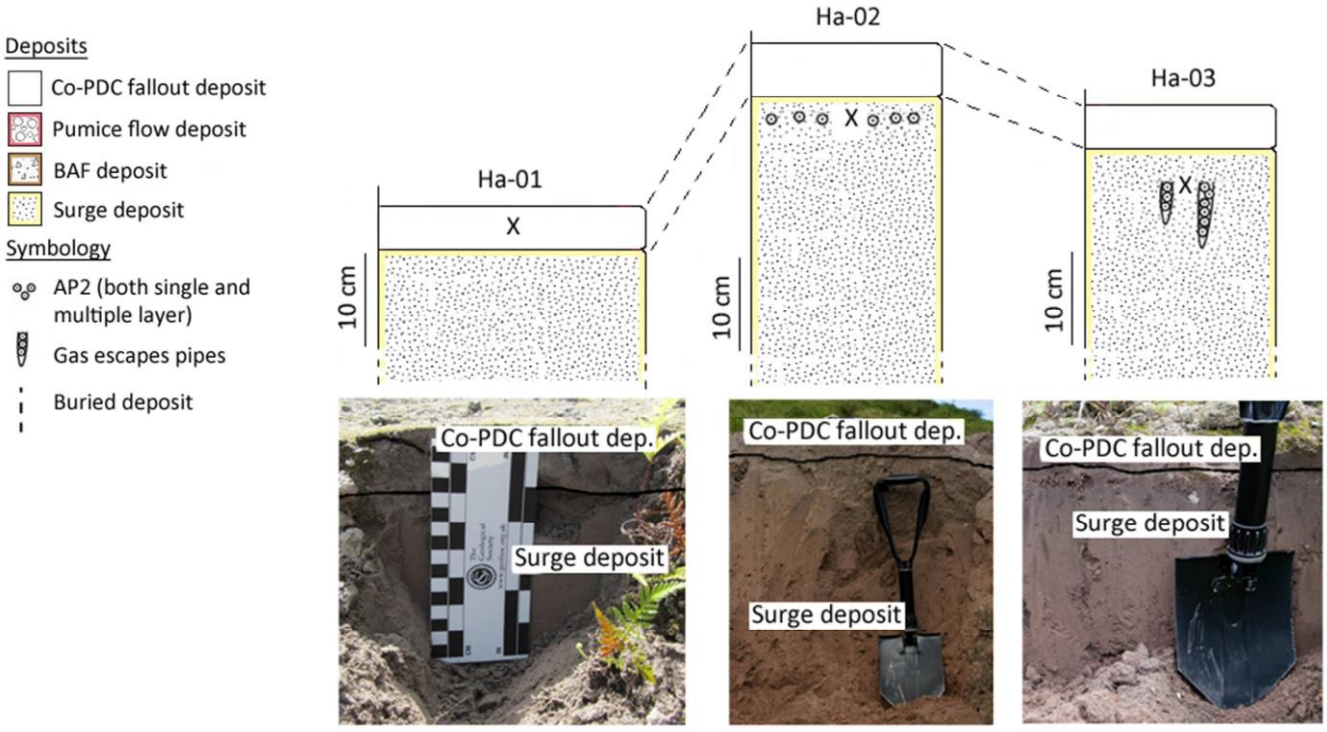

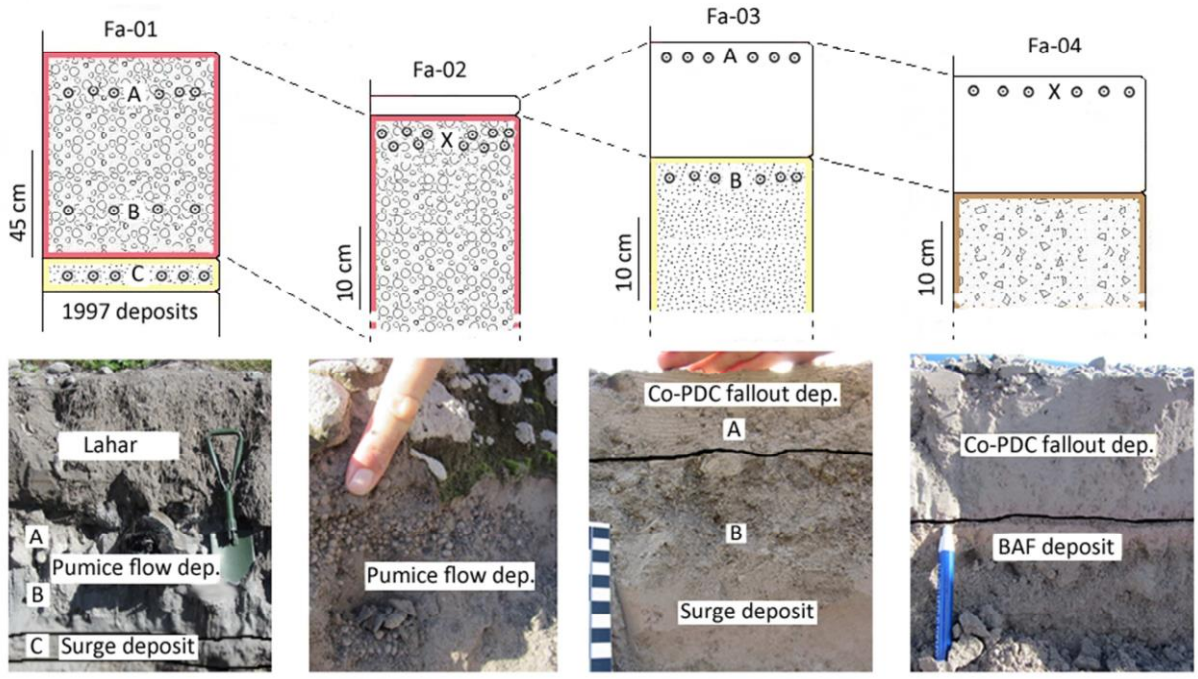

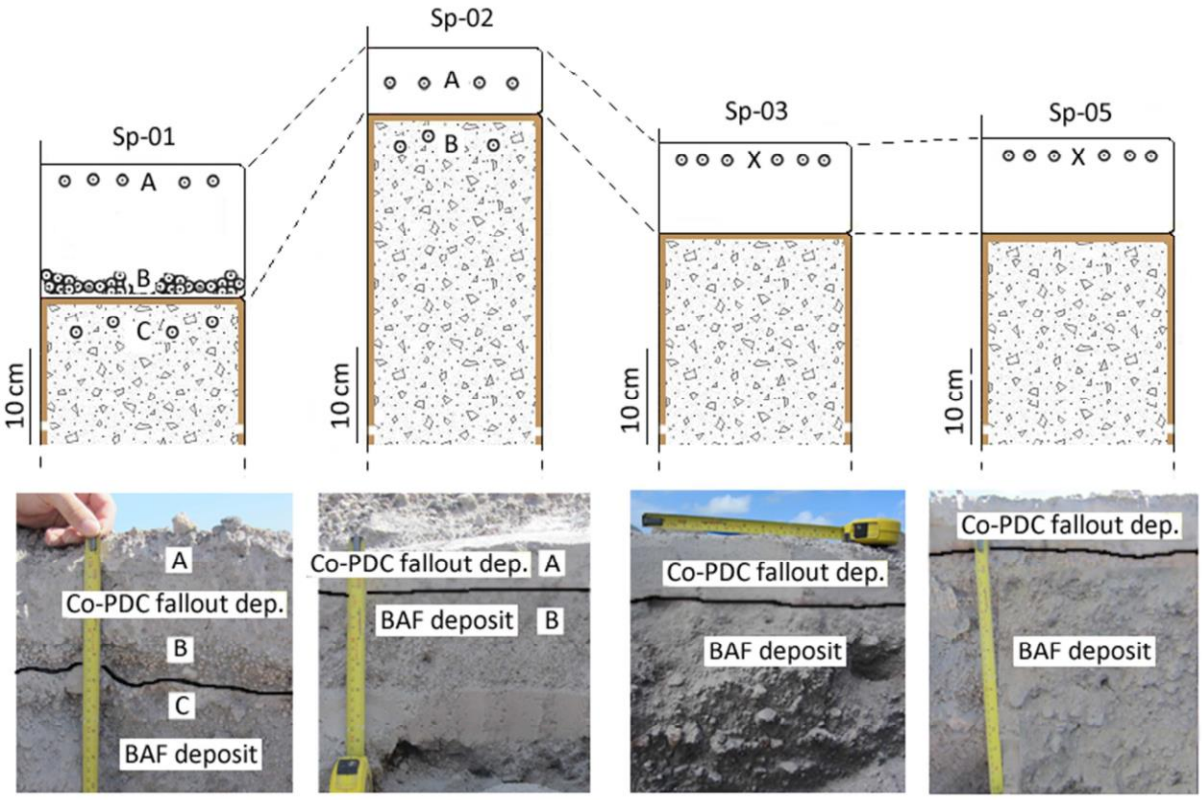
Sp-01
Sp-02
Sp-03
Sp-05
A
B
C
X
10 cm
A
Co-PDC fallout dep.
B
C
BAF deposit
Co-PDC fallout dep.
A
BAF deposit
B
Co-PDC fallout dep.
BAF deposit
Co-PDC fallout dep.
BAF deposit

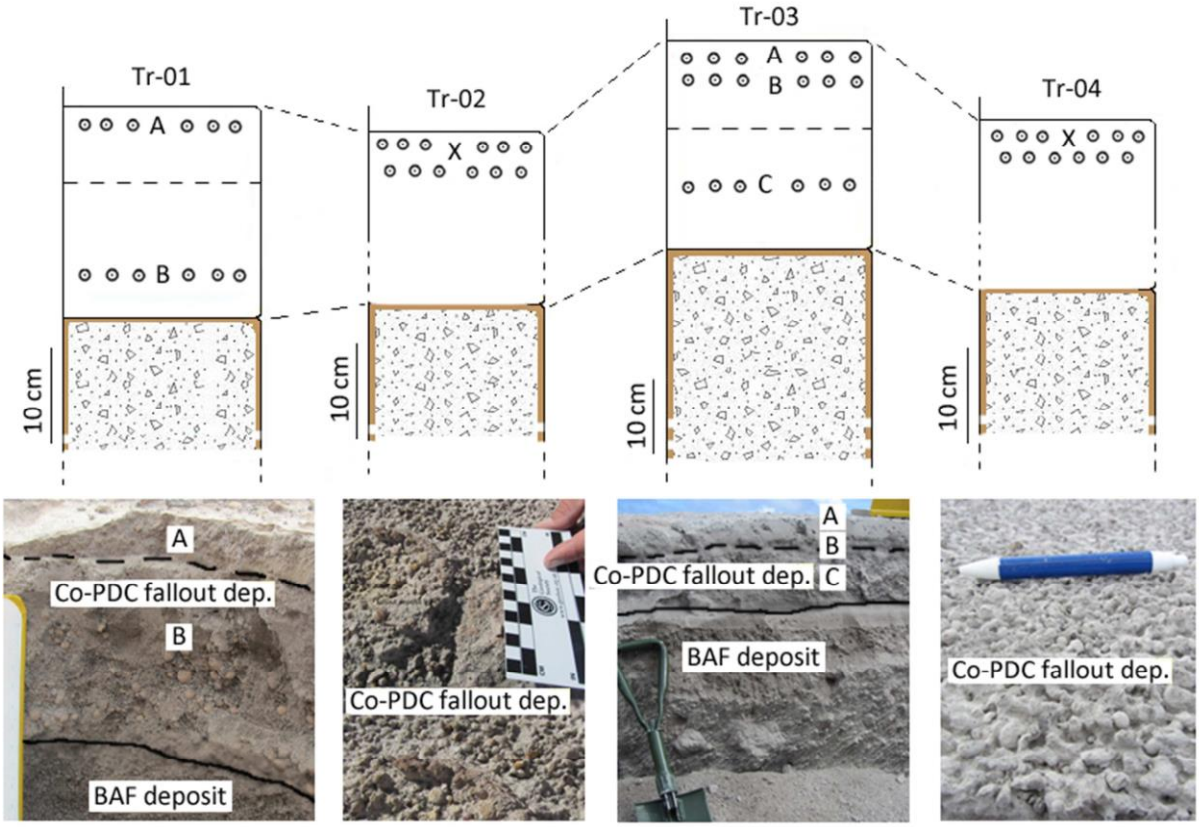
Tr-01
Tr-02
Tr-03
Tr-04
A
B
C
X
10 cm
A
Co-PDC fallout dep.
B
BAF deposit
Co-PDC fallout dep.
A
B
Co-PDC fallout dep.
C
BAF deposit
Co-PDC fallout dep.

Appendix II

AGGREGATE TEXTURES

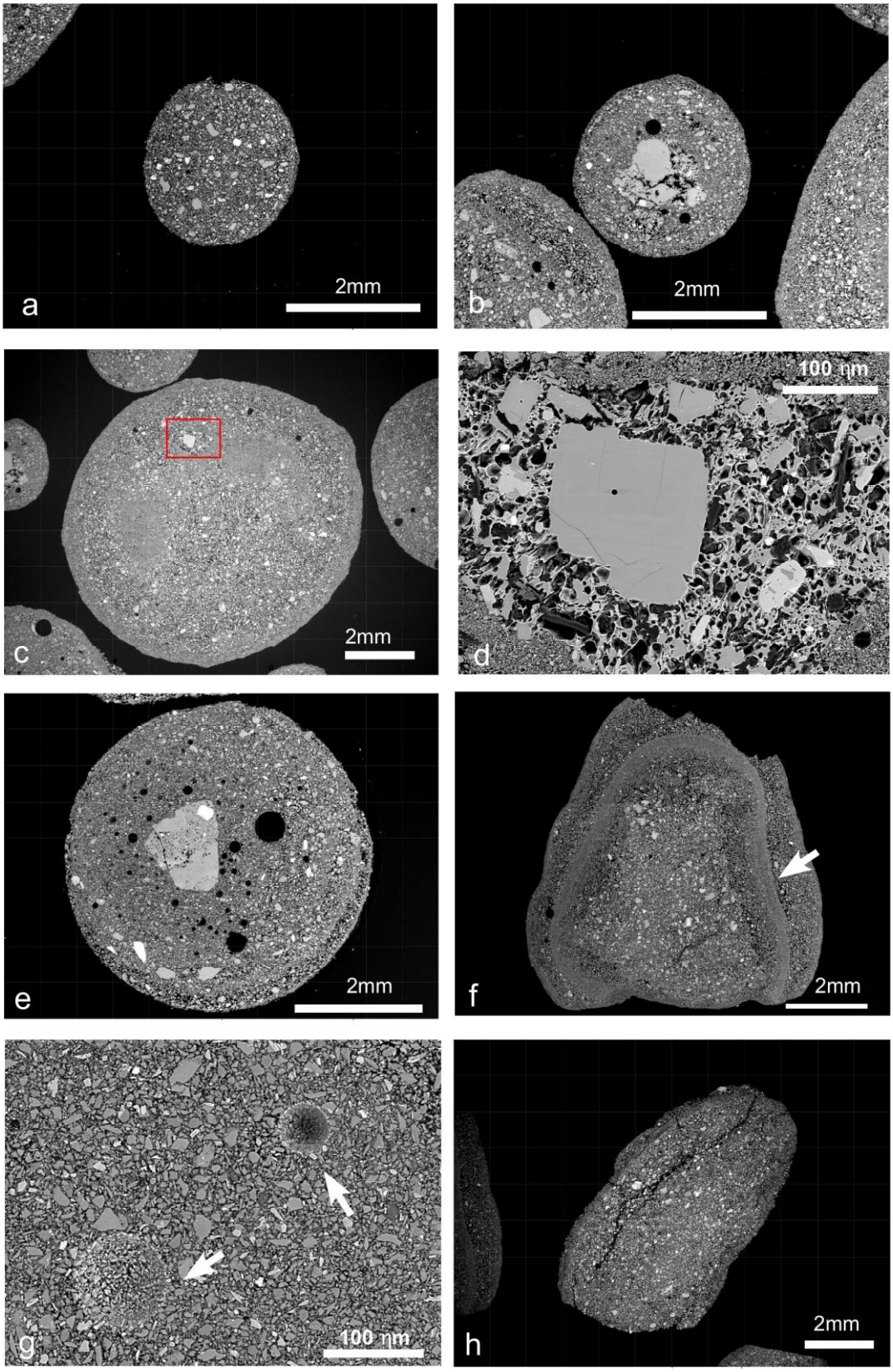

Fig. II.1. SEM backscattered images of cross section of aggregates: a) single-layer AP2 (co-PDC fallout deposit; Sp-03 in Appendix I); b) single-layer AP2 with crystal core (co-PDC fallout deposit; Sp-02A in

Appendix I); c) single-layer AP2 with irregular, fine-grained core (co-PDC fallout deposit; Sp-03 in Appendix I); d) close up of pumice fragment in single-layer AP2 shown in c) (area enclosed in the red rectangle of fig. c))); e) multiple-layer AP2 with crystalline core (co-PDC fallout deposit; Tr-04 in Appendix I; black circles are due to resin bubbles); f) multiple-layer AP2 partially eroded: an unusual intermediate size sub-layer can be seen between the fine-grained layer 1 (marked by an arrow) and the core (co-PDC fallout deposit; Fa-02 in Appendix I); g) primary spherical cavities in AP2 (marked by arrows; co-PDC fallout deposit; Tr-02 in Appendix I); h) oblate AP2 (co-PDC fallout deposit; Tr-02 in Appendix I).

REFERENCES

Bagheri G and Bonadonna C (2016) Aerodynamics of Volcanic Particles: Characterization of Size, Shape, and Settling Velocity, In: Volcanic Ash, 1st Edition, Editors: Mackie, Cashman, Ricketts, Rust and Watson, Elsevier, ISBN: 9780081004050, pp. 300

Bagheri G, Rossi E, Biass S, Bonadonna C (2016) Timing and nature of volcanic particle clusters based on field and numerical investigations, Journal of Volcanology and Geothermal Research, http://dx.doi.org/10.1016/j.jvolgeores.2016.09.009

Bonadonna, C., Mayberry, G. C., Calder, E. S. et al. (2002). Tephra fallout in the eruption of Soufriere Hills Volcano, Montserrat. In: Druitt, T. H. & Kokelaar, B. P., eds. *The Eruption of Soufriere Hills Volcano, Montserrat, from 1995 to 1999.* Geological Society of London, Memoirs, 21, p. 483-516.

Bonadonna, C., Genco, R., Gouhier, M., Pistolesi, M., Cioni, R., Alfano, F., Hoskuldsson, A., Ripepe, M. (2011). Tephra sedimentation during the 2010 Eyjafjallajökull eruption (Iceland) from deposit, radar, and satellite observations, *Journal of Geophysical Research*, 116. doi: 10.1029/2011JB008462.

Bonadonna, C., R. Cioni, M. Pistolesi, M. Elissondo, and V. Baumann (2015), Sedimentation of longlasting wind-affected volcanic plumes: the example of the 2011 rhyolitic Cordón Caulle eruption, Chile. Bulletin of Volcanology, doi: 10.1007/s00445-015-0900-8

Bonadonna, C. and Costa, A. (2012). Estimating the volume of tephra deposits: A new simple strategy. *Geology*, doi: 10.1130/G32769.1.

Brazier S, Davis AN, Sigurdsson H, Sparks RSJ (1982) Fallout and Deposition of Volcanic Ash During the 1979 Explosive Eruption of the Soufrière of St-Vincent. Journal of Volcanology and Geothermal Research 14(3-4):335-359

Brazier S, Sparks RSJ, Carey SN, Sigurdsson H, Westgate JA (1983) Bimodal grain-size distribution and secondary thickening in air-fall ash layers. Nature 301(5896):115-119

Brown, R.J., Branney, M.J. (2004). Event-stratigraphy of a caldera-forming PDC deposit eruption on Tenerife: the 273 ka Poris formation. *Bulletin of Volcanology*, 66, p.392–416.

Brown, R.J., Branney, M.J., Maher, C., Davila-Harris, P., (2010) Origin of accretionary lapilli within ground-hugging density currents: evidence from pyroclastic couplets on Tenerife. *Geological Society of America Bulletin*, 122, p. 305-320.

Brown, R.J., Bonadonna, C., Durant, A.J. (2012). A review of volcanic ash aggregation. *Physics and Chemistry of the Earth*, 45-46, p. 65-78.

Carey, S.N., Sigurdsson, H. (1982). Influence of particle aggregation on deposition of distal tephra from the May 18 1980 eruption of Mount St. Helens volcano. *Journal of Geophysical Research*, 87, p.7061-7072.

878 Cheng, R.J. (1973). Photomicroscopical investigation of fragmentation of hydrometeors in the
879 laboratory. The Microscope, 21, 3, 149—160.
880 Cheng, H.C. and Lemlich, R. (1983). Errors in the Measurement of Bubble Size Distribution in Foam. Ind.
881 Eng. Chem. Fundam., 22, 105–109.
882 Cole, P.D., Calder, E.S., et al. (2002). Deposit from dome-collapse and fountain-collapse pyroclastic
883 flows at Soufrière Hills Volcano, Montserrat. In: Druitt, T. H. & Kokelaar, B. P., eds. *The Eruption of*
884 *Soufriere Hills Volcano, Montserrat, from 1995 to 1999.* Geological Society of London, Memoirs, 21,
885 p. 231-262.
886 Cole, P.D., Smith, P.J., Stinton, A.J., Odbert, H.M., Bernstein, M., Komorowski, J-C., & Stewart, R.
887 (2014a). Vulcanian Explosions at Soufriere Hills Volcano between 2008 and 2010. In: Wadge G.,
888 Robertson R., & Voight B. eds. The *Eruption of Soufrière Hills Volcano, Montserrat, from 2000 to*
889 *2010.* Geological Society, London, Memoirs, 39, p.93-111.
890 Cole, P.D., Smith, P.J., Komorowski, J-C., Alfano F., Bonadonna C., Stinton A.J., Christopher T., Odbert,
891 H.M., & Loughlin, S. (2014b). Ash venting occurring both prior to and during lava extrusion at
892 Soufrière Hills Volcano, Montserrat, from 2005 to 2010. *The Eruption of Soufriere Hills Volcano,*
893 *Montserrat, from 2000 to 2010*. Geological Society, London, Memoirs, 39, p. 71-92.
894 Cole, P.D., Stinton, A.J., Odbert, H.M., Bonadonna, C., Stewart, R.C. (2015). An inclined Vulcanian
895 explosion and associated products. *Journal of the Geological Society*, 172, 287-293, doi:
896 10.1144/jgs2014-099.
897 Costa, A., Folch, A., Macedonio, G. (2010). A model for wet aggregation of ash particles in volcanic
898 plumes and clouds: 1. Theoretical formulation. *Journal of Geophysical Research*, 115, B09201.
899 doi:10.1029/2009JB007175.
900 Durant, AJ (2015) RESEARCH FOCUS: Toward a realistic formulation of fine-ash lifetime in volcanic
901 clouds, Geology, v. 43, p. 271-272, doi:10.1130/focus032015.1
902 Durant, A.J., D.A. Swanson, and W.I. Rose (2002), Accretionary Lapilli Beds in the Keanakako'i Ash:
903 Footprint Bearing Beds not 1790 in Age, Eos Trans. AGU, 83(47), Fall Meet. Suppl., Abstr. V12B-
904 1433
905 Durant, A.J., and R. A. Shaw (2005), Evaporation Freezing by Contact Nucleation Inside-Out, Geophys.
906 Res.Lett., 32, L20814, doi:10.1029/2005GL024175.
907 Durant, A.J., Rose, W.I., Sarna-Wojcicki, A.M., Carey, S. Volentik, A.C.M. (2009). Hydrometeorenhanced
908 tephra sedimentation: Constraints from the, 18 May, 1980eruption of Mount St. Helens. *Journal of*
909 *Geophysical Research,* 114. doi: 10.1029/2008JB005756.
910 Druitt, T.H., Young, S.R., et al. (2002). Episodes of cyclic Vulcanian explosive activity with fountain
911 collapse at Soufrière Hills Volcano, Montserrat. In: Druitt, T. H. & Kokelaar, B. P., eds. *The Eruption*

912 *of Soufriere Hills Volcano, Montserrat, from 1995 to 1999.* Geological Society of London, Memoirs,
913 21, p. 281-306.
914 Ennis BJ, Tardos G, Pfeffer R (1991) A microlevel-based characterization of granulation phenomena.
915 Powder Technol 65:257–272
916 Gilbert, J.S., Lane, S.J. (1994). The origin of accretionary lapilli. *Bulletin of Volcanology*, 56, p. 398-411.
917 Herzog M, Graf HF, Textor C and Oberhuber JM (1998) The effect of phase changes of water on the
918 developments of volcanic plumes, Journal of Volcanology and Geothermal Research, 87, 55.74
919 Houze (2014) Cloud Dynamics, Academic Press, ISBN: 9780123742667, 496 pages
920 James, M.R., Lane, S.J., Gilbert, J.S. (2003). Density, construction, and drag coefficient of electrostatic
921 volcanic ash aggregates*. Journal of Geophysical Research*, 108, 2435.
922 List R., Murray W. A. and Dyck C. (1972) Air bubbles in hailstones, Journal of the Atmospheric
923 Sciences, Vol. 29, No. 5, p. 916 - 20.
924 Mangan, M.T., Cashman, K.V. and Newman, S. (1993). Vesiculation of basaltic magma during eruption.
925 *Geology*, 21, p. 157-160.
926 Mayberry, G.C., Rose, W.I. and Bluth, G.J.S. (2002). Dynamics of volcanic and meteorological clouds
927 produced on 26 December (Boxing Day) 1997 at Soufriere Hills Volcano, Montserrat. In: Druitt, T.H.
928 & Kokelaar, B.P., eds. *The Eruption of Soufriere Hills Volcano, Montserrat, from 1995 to 1999.*
929 Geological Society of London, Memoirs, 21, p. 539-555.
930 Melnik, O., and R. S. J. Sparks (2002), Dynamics of magma ascent and lava extrusion at Soufriere Hills
931 Volcano, Montserrat, in The Eruption of the Soufriere Hills Volcano, Montserrat From 1995 to 1999,
932 edited by T. H. Druitt and B. P. Kokelaar, Mem. Geol. Soc. London, 21, 153–171.
933 Mueller, S.B., Kueppers, U., Ayris, P., Jacob, M., Dingwell, D.B., (2016) Experimental volcanic ash
934 aggregation: Internal structuring of accretionary lapilli and the role of liquid bonding, Earth and
935 Planetary Science Letters, Volume 433, Pages 232–240
936 Pyle, D. M. (1989). The thickness, volume and grainsize of tephra fall deposits, *Bulletin of Volcanology*,
937 51, p.1-15.
938 Ritchie, L.J., Cole, P.D., Sparks, R.S.J. (2002). Sedimentology of deposits from the pyroclastic density
939 currents of 26 December 1997 at Soufrière Hills Volcano, Montserrat. In: Druitt, T.H. & Kokelaar,
940 B.P., eds. *The Eruption of Soufriere Hills Volcano, Montserrat, from 1995 to 1999.* Geological Society
941 of London, Memoirs, 21, p. 435-456.
942 Roduit, N. (2006) JMicroVision: Image analysis toolbox for measuring and quantifying components of
943 high-definition images. Version 1.2.2. http://www.jmicrovision.com
944 Rose, W. I., D. J. Delene, D. J. Schneider, G. J. S., Bluth, A. J. Krueger, I. Sprod, C. McKee, H. L, Davies
945 and G. G. J. Ernst (1995) Ice in the 1994 Rabaul eruption cloud: implications for volcano hazard and
946 atmospheric effects, Nature, 375: 477-479

947 Rose WI, Durant AJ (2011) Fate of volcanic ash: Aggregation and fallout. Geology 39(9):895-896
948 Schumacher R (1994) A reappraisal of Mount St. Helens ash clustersdepositional model from
949 experimental observation. J Volcanol Geotherm Res 59:253–260
950 Schumacher R, Schmincke H-U (1995) Models for the origin of accretionary lapilli. Bull Volcanol 56:626–
951 639
952 Scolamacchia T., J. L. Macías, M. F. Sheridan, S. R. Hughes (2005) Morphology of ash aggregates from
953 wet pyroclastic surges of the 1982 eruption of El Chichón Volcano, Mexico, Bulletin of
954 Volcanology, 68 (2) , pp 171-200
955 Sparks, R.S.J., Bursik, M.I., Carey, S.N., Gilbert, J.S., Glaze, L.S., Sigurdsson, H., Woods, A.W. (1997)
956 Volcanic Plumes. *John Wiley & Sons*, Chichester, p.574.
957 Stinton, A.J., Cole, P.D., Odbert, H.M., et al. (2014a). Dome growth and valley fill during Phase 5 (8
958 October 2009 – 11 February 2010) at the Soufrière Hills Volcano, Montserrat. In G. Wadge, B.
959 Voight, & R. Robertson, eds. *The Eruption of Soufriere Hills Volcano, Montserrat, from 2000 to 2010*.
960 Geological Society, London, Memoirs, 39, p. 113-131.
961 Stinton, A.J., Cole, P.D., Stewart, R.C., et al. (2014b). The 11 February 2010 partial dome collapse at
962 Soufriere Hills Volcano, Montserrat. In G. Wadge, B. Voight, & R. Robertson, eds. *The Eruption of*
963 *Soufriere Hills Volcano, Montserrat, from 2000 to 2010*. Geological Society, London, Memoirs, 39,
964 p. 133-152.
965 Tabazadeh, A., and R. P. Turco (1993) Stratospheric chlorine injection by volcanic eruptions: HCl
966 scavenging and implications for ozone, Science,260,1082–1086
967 Taddeucci J, Scarlato P, Montanaro C, Cimarelli C, Del Bello E, Freda C, Andronico D, Gudmundsson MT,
968 Dingwell DB (2011) Aggregation-dominated ash settling from the Eyjafjallajokull volcanic cloud
969 illuminated by field and laboratory high-speed imaging. Geology 39(9):891-894
970 Textor C., Graf H.F., Herzog M., Oberhuber J. M. (2003). Injection of gases into the stratosphere by
971 explosive volcanic eruptions. Journal of Geophysical Research: Atmospheres 108(D19),
972 doi:10.1029/2002JD002987
973 Van Eaton, A.R, Wilson, C.J.N. (2013). The nature, origins and distribution of ash aggregates in a large-
974 scale wet eruption deposit: Oruanui, New Zealand. *Journal of Volcanology and Geothermal*
975 *Research,* 250, p.129-154.
976 Van Eaton, AR, Muirhead, JD, Wilson, CJN, Cimarelli, C (2012) Growth of volcanic ash aggregates in the
977 presence of liquid water and ice: an experimental approach, *Bulletin of Volcanology*, 74, 9, pp 1963-
978 1984

Watanabe, K., Ono, K., Sakaguchi, K., Takada, A., Hoshizumi, H. (1999). Co-pyroclastic density current ash-fall deposits of the 1991 eruptions of Fugen-dake, Unzen Volcano, Japan. *Journal of Volcanology and Geothermal Research*, 89, p. 95-112.

Wilson, C.J.N. (2001). The, 26.5 ka Oruanui eruption, New Zealand: an introduction and overview. *Journal of Volcanology and Geothermal Research*, 112, p. 133-174.

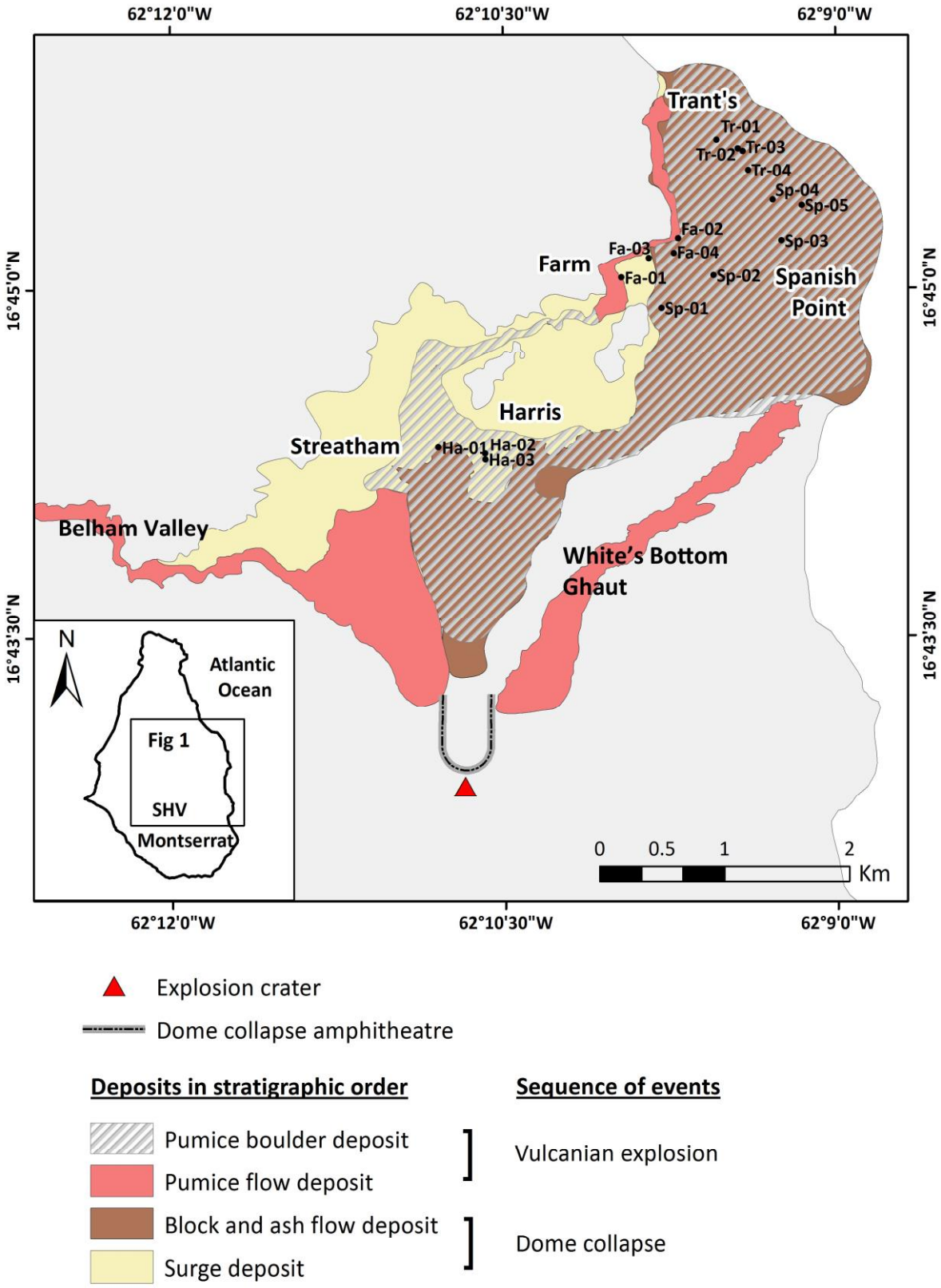

984

985 **Figure 1**: Map showing selected products of the dome collapse of 11 February 2010 deposited on the
986 northern flank of the Soufriere Hills Volcano, Montserrat (adjusted from Cole et al. 2015). Inset shows
987 the location of Fig 1 on the island. Location and name of samples used in this work is also shown.

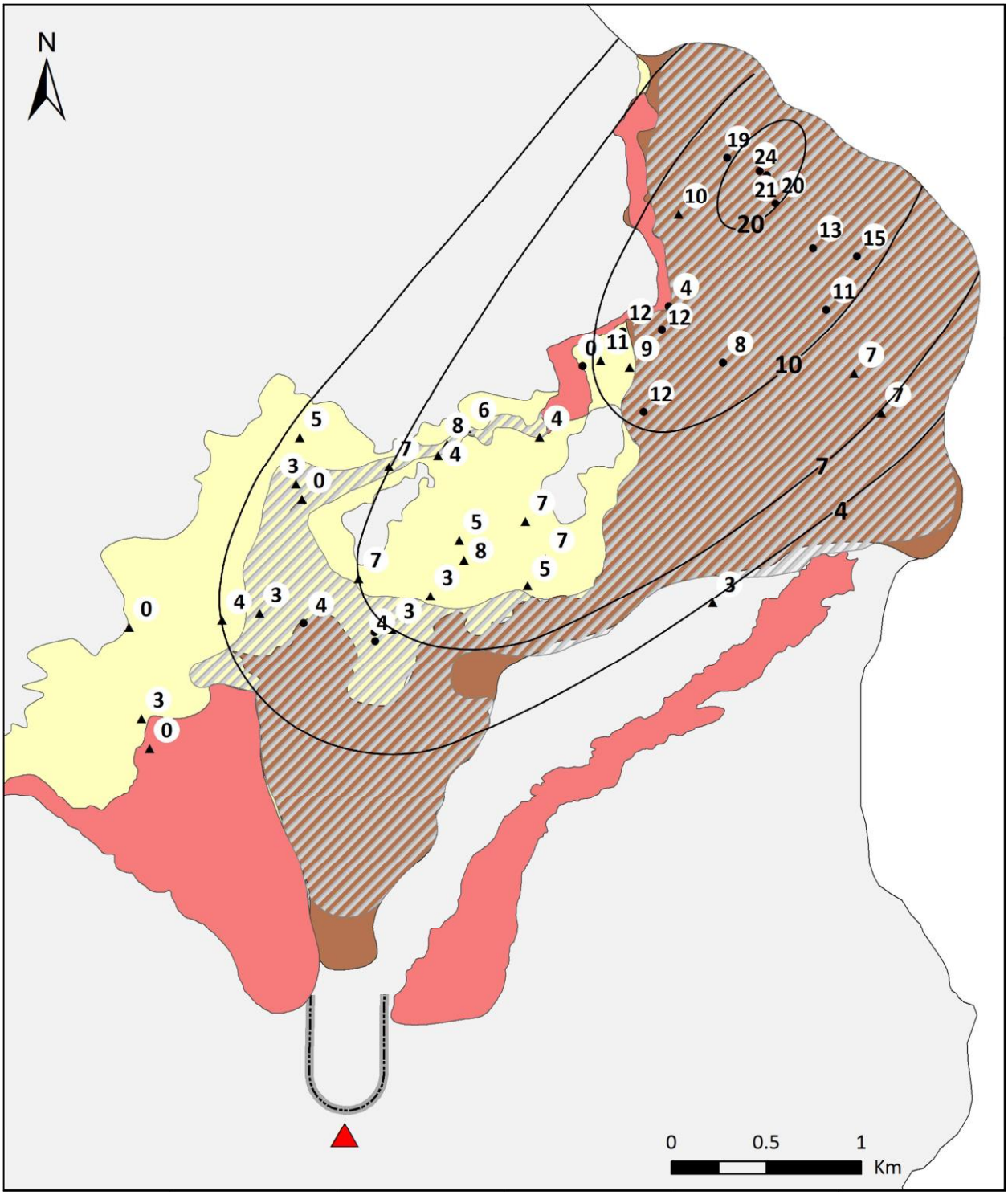

Figure 2: Isopach map for the co-PDC fallout deposit (cm) associated with the 11 February 2010 dome collapse: 28 sites (triangles) are from Stinton et al. (2014), and 16 sites (circles) are from this study. Legend as in Fig. 1.

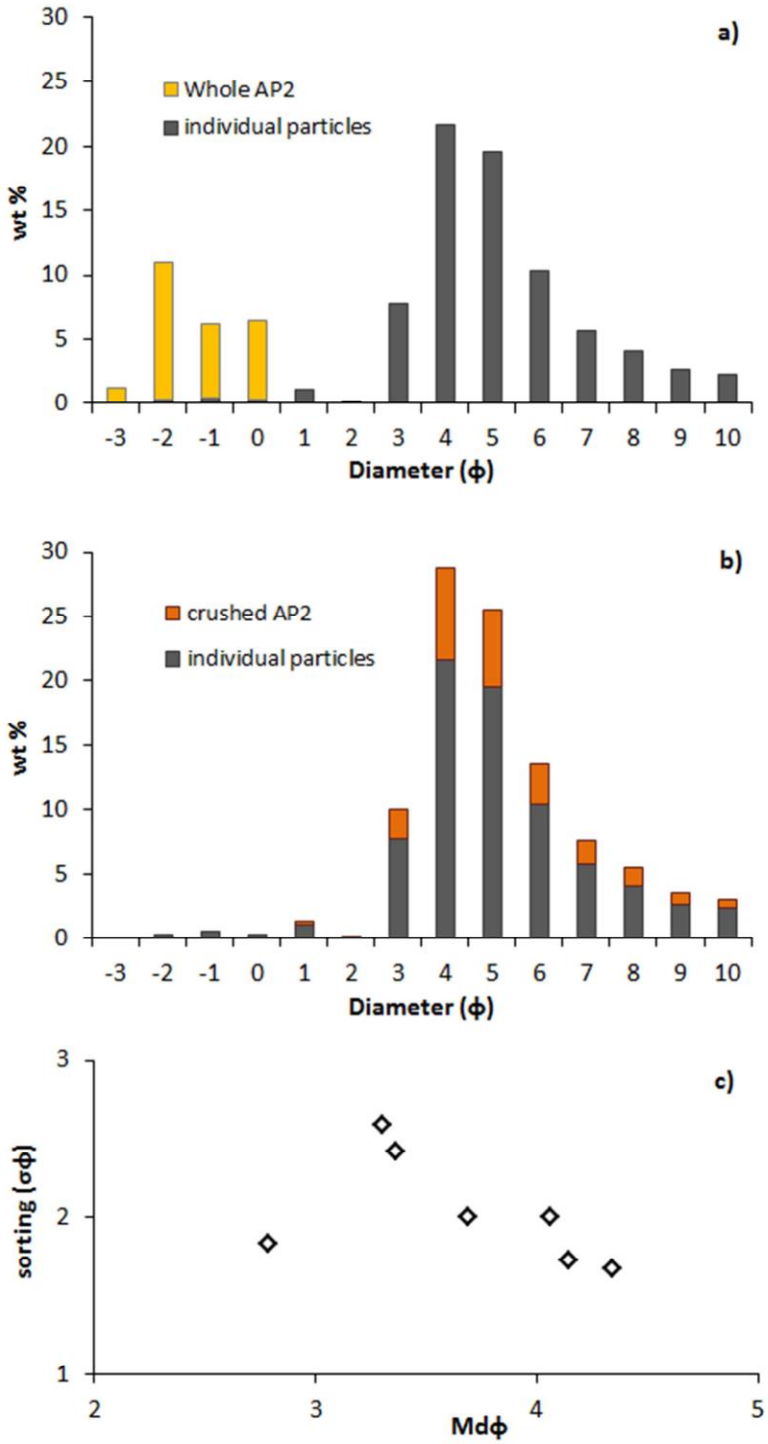

995
996
997
998 **Figure 3**: Grain size distribution of the co-PDC fallout sample Tr-02 in Appendix I with a) whole AP2
999 aggregates and b) crushed AP2 aggregates. c) Mdphi versus sorting of all co-PDC fallout samples (with
1000 crushed AP2s).
1001
1002
1003

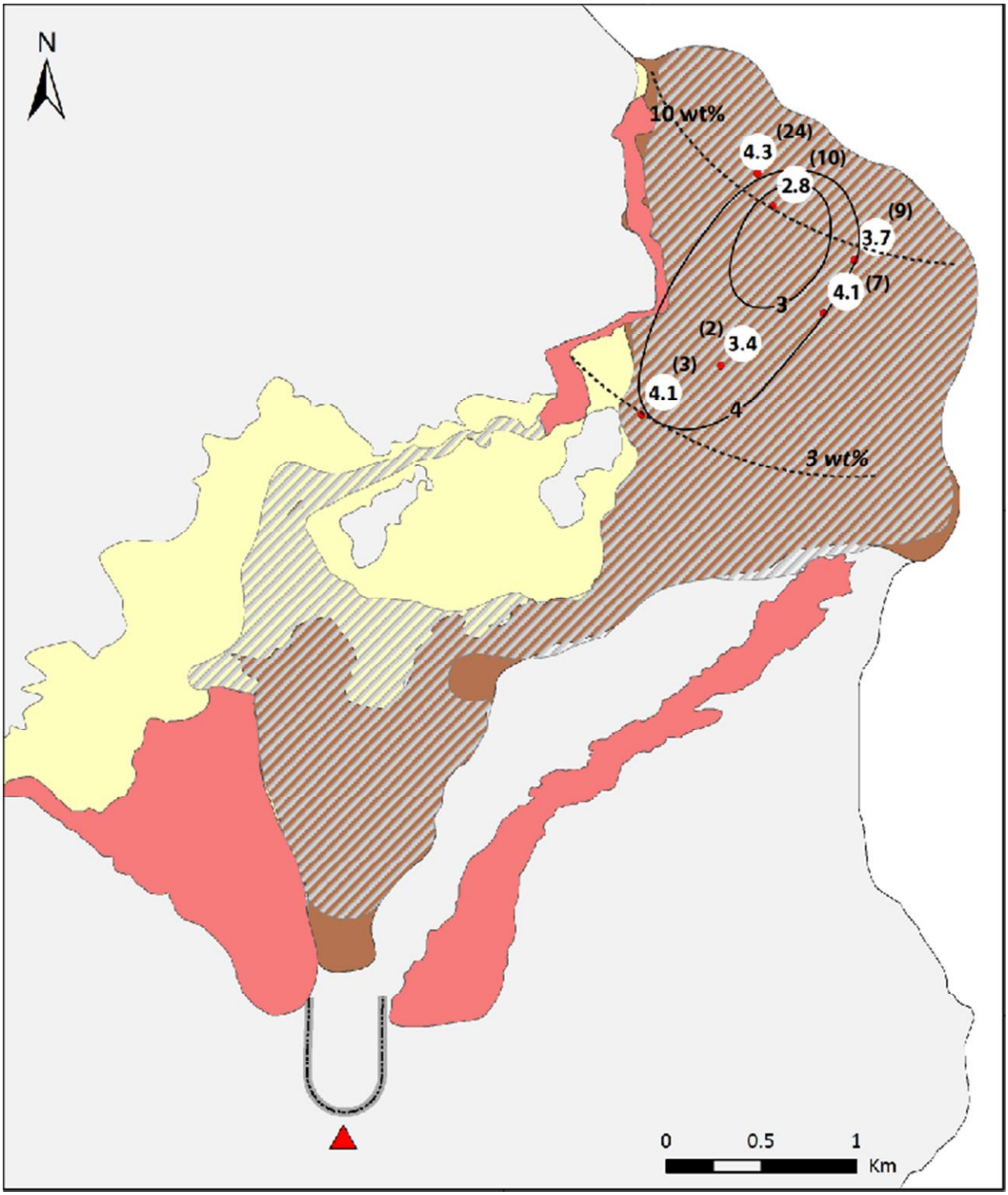

Figure 4: Mdphi map for the co-PDC fallout deposit (in ϕ); values of aggregate abundance (in brackets; wt%) and isograde of same abundance (dashed lines; wt%) are also shown. Mdphi is calculated for crushed AP2s.

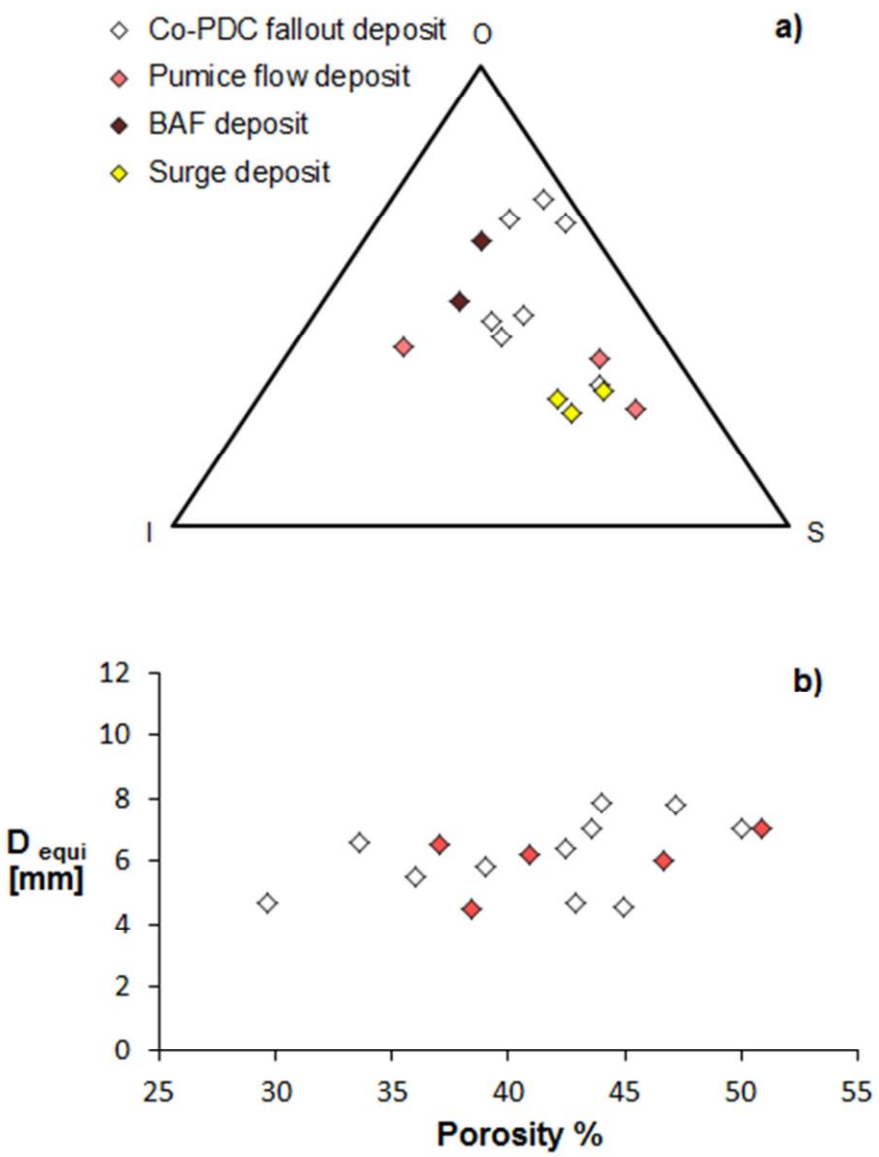

Figure 5: a) Morphology of AP2s (O: Oblate, S: Spherical and I: Irregular) in relation to their relative abundance (wt%) in the different deposits; b) AP2 porosity with respect to their equivalent diameter. White, red, brown and yellow diamonds indicate aggregates sampled from co-PDC fallout deposit, pumice flow deposit, BAF deposit and surge deposit, respectively. The equivalent diameter of the aggregate was calculated from the volume of the aggregate as $\mathbf{D_{equi}}$ $\sqrt{\frac{3}{4}V/\pi}$, with V being the aggregate volume.

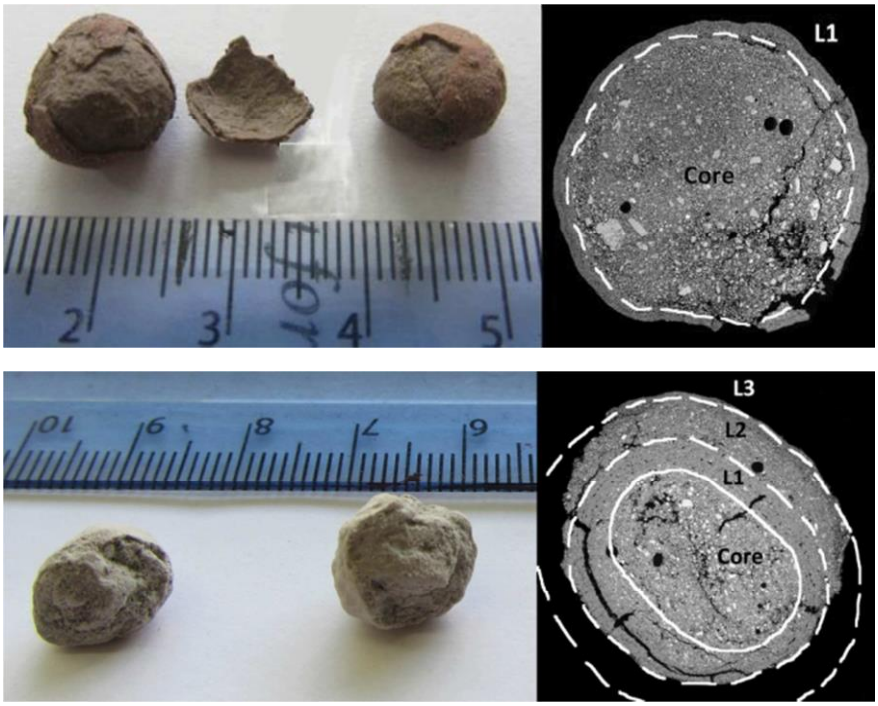

Figure 6: Still photos and SEM cross-sections (magnification of 64 x, 8 mm WD) of a) a single-layer AP2 (from co-PDC fallout deposit SP-02 in Appendix I) and b) a multiple-layer AP2 (from pumice-flow deposit Fa-02 in Appendix I).

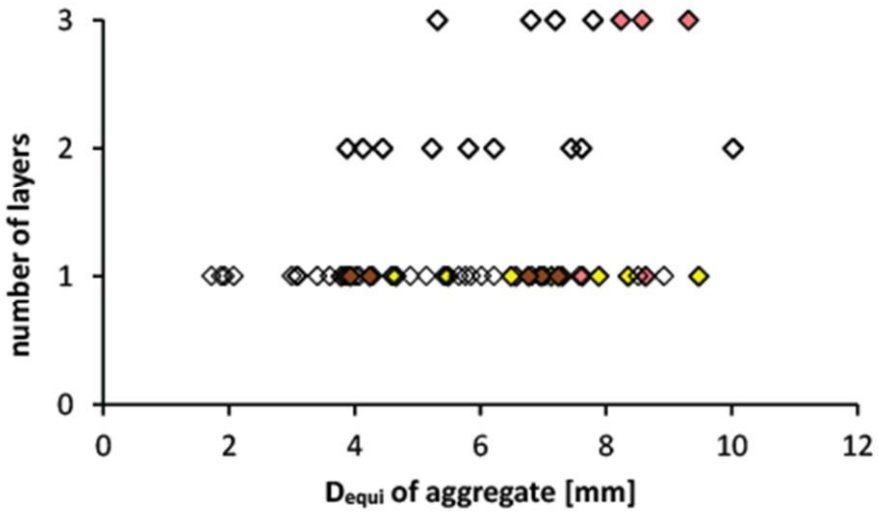

Figure 7: Number of layers for AP2s correlated with their size and the type of deposit they were sampled from. Legend and equivalent diameter as in Fig. 5.

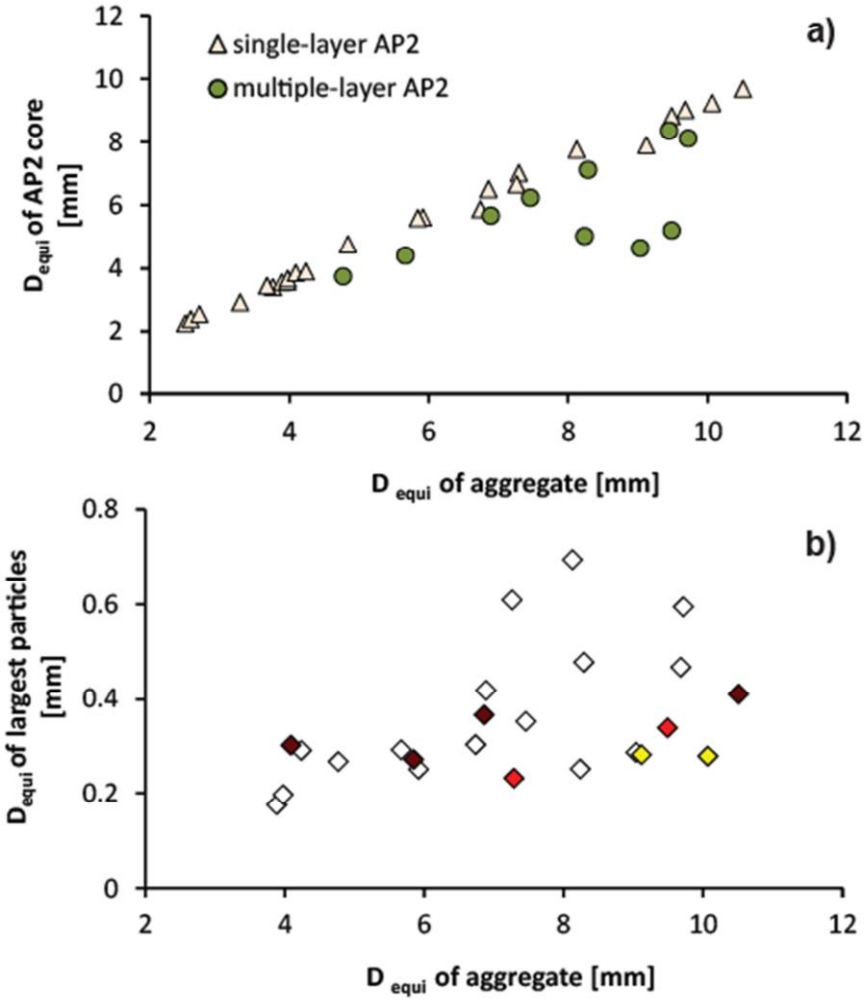

1035

1036 **Figure 8**: a) Core diameter (mm) and b) diameter of the largest particles in the aggregate core (mm)

1037 with respect to the equivalent diameter of the aggregate (mm). Legend for Fig 8b as in Fig. 5.

1038

1039

1040

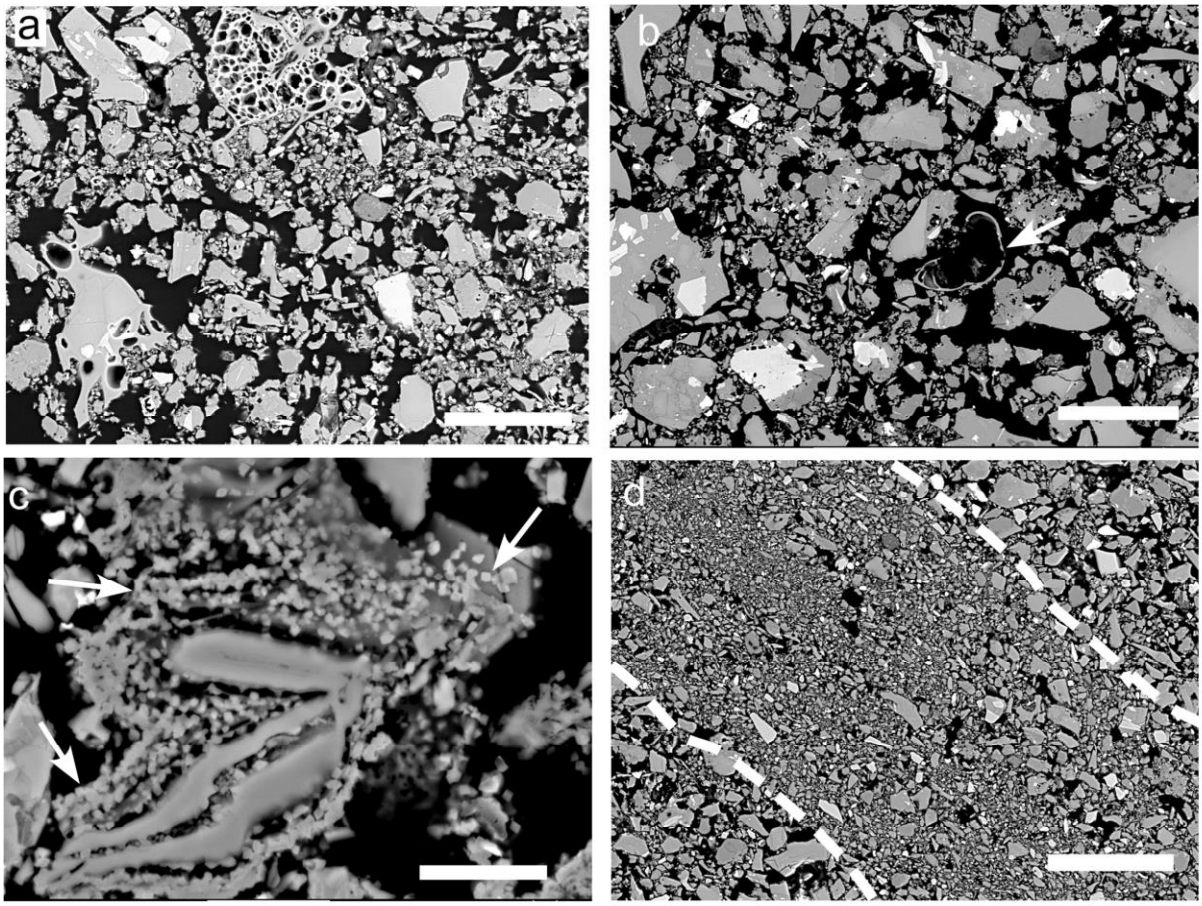

1041

1042

1043 **Figure 9**. SEM Back Scattered Images of internal textures of aggregates: a) typical ash grains in
1044 aggregate (co-PDC, Tr-02 location in Appendix I), b) Foraminifera shell (marked by the arrow)
1045 embedded in the core of aggregate (co-PDC, Tr-02 location in Appendix I), c) cubic salt crystals matrix
1046 (marked by arrows) surrounding pyroclastic fragments (core) in same aggregate as b), d) fine-grained
1047 layer 1 embedded in between coarser core (bottom left of the figure) and layer 2 in a multiple layer
1048 aggregate (pumice-flow deposit, location Fa-01 in Appendix I); layer limits are outlined by dashed lines.
1049 White bar indicates 10 μm in figure c) and 100 μm in figures a), b) and d.

1050

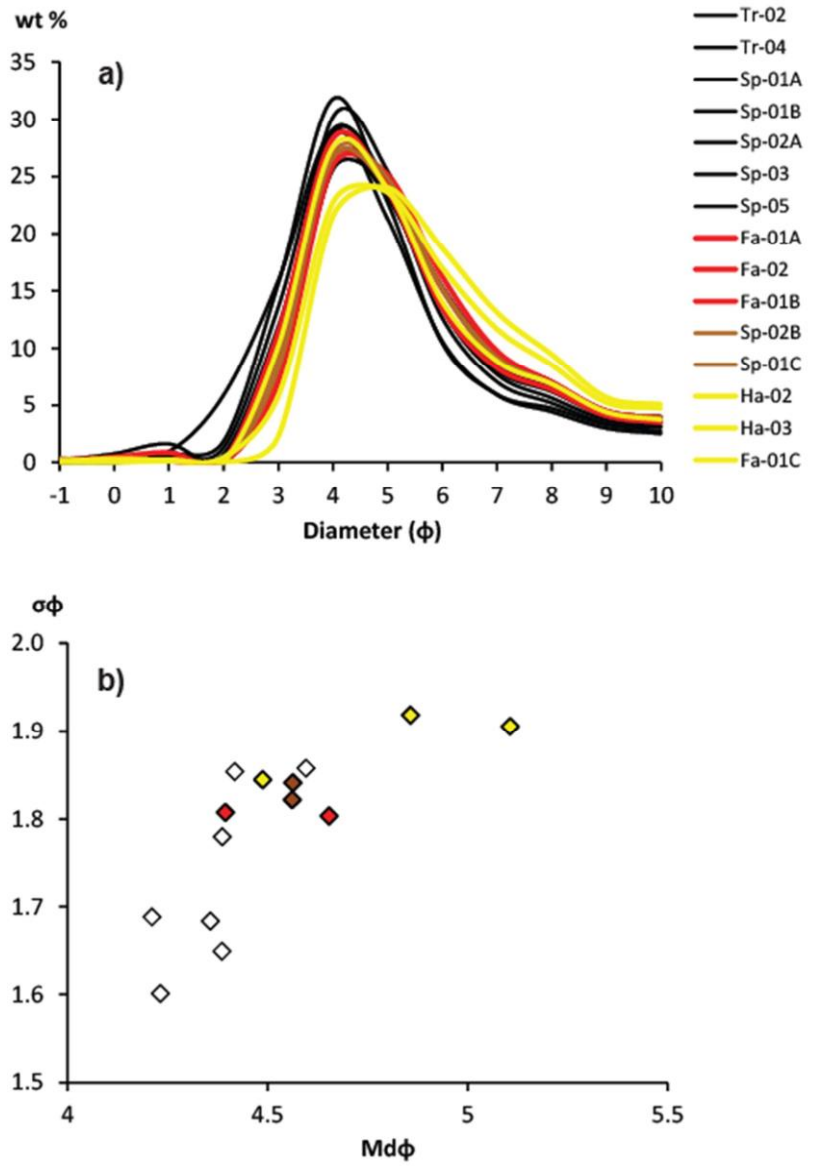

1051
1052

1053 **Figure 10**: a) Internal grain-size distribution and b) Mdϕ versus sorting for crushed AP2s from different

1054 deposits. Deposit legend as in Fig. 5.

1055

1056

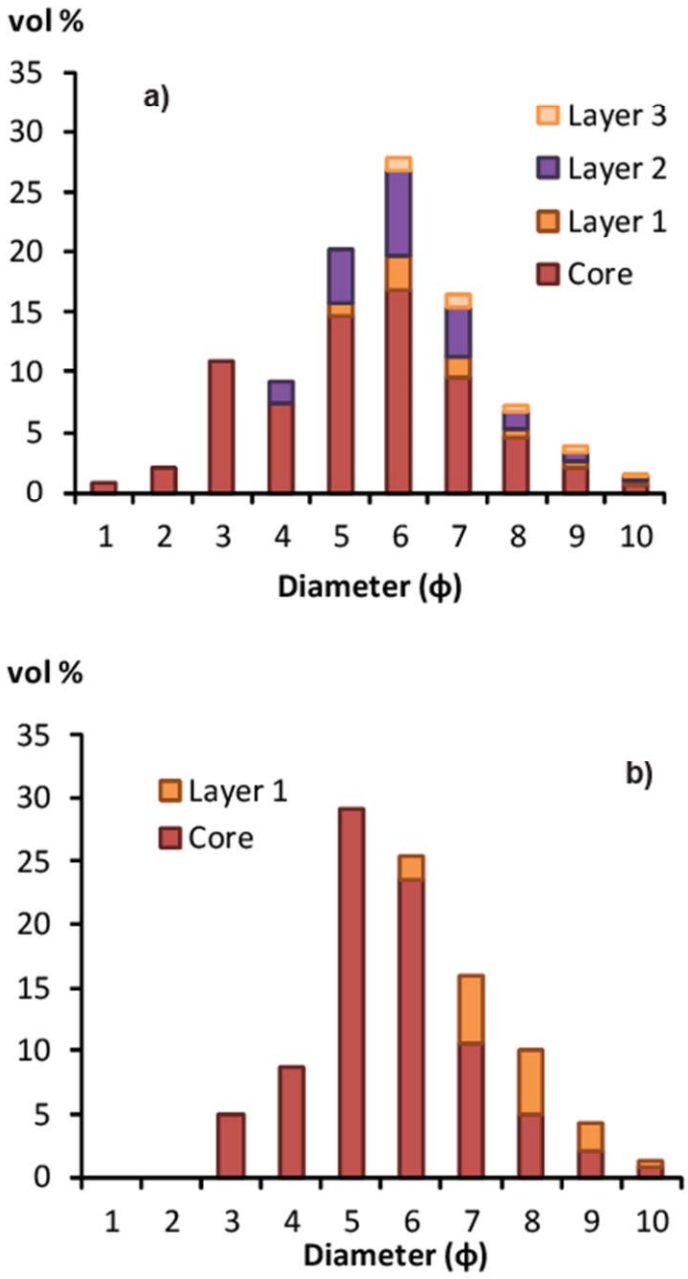

1057

1058 **Figure 11**: 3D particle size distribution for a) AP2 Sp-03a and b) AP2 Sp-03h in Appendix I.

1059

1060

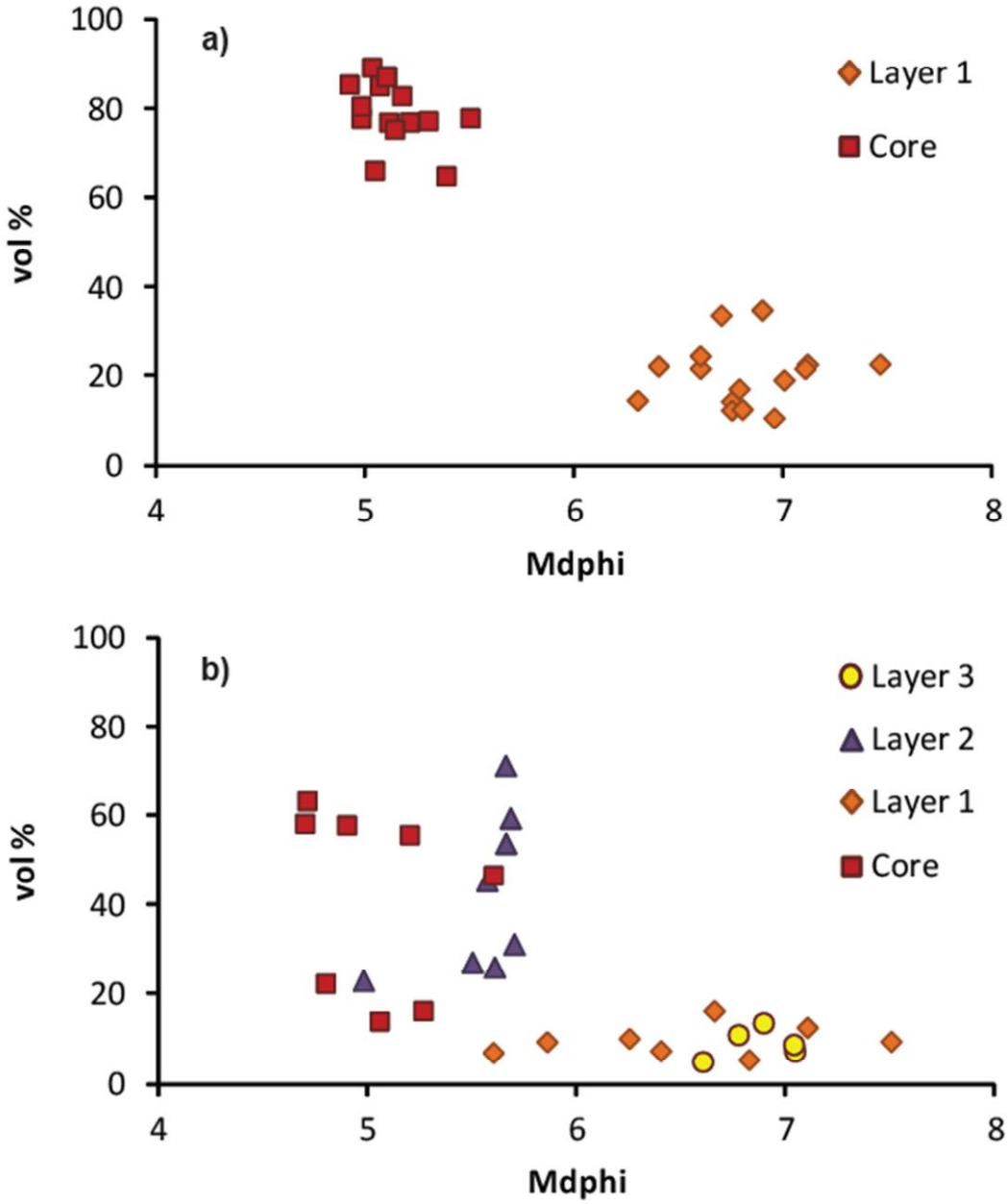

Figure 12: Mdϕ versus volume fraction (vol%) for a) single-layer AP2s and b) multiple-layer AP2s.

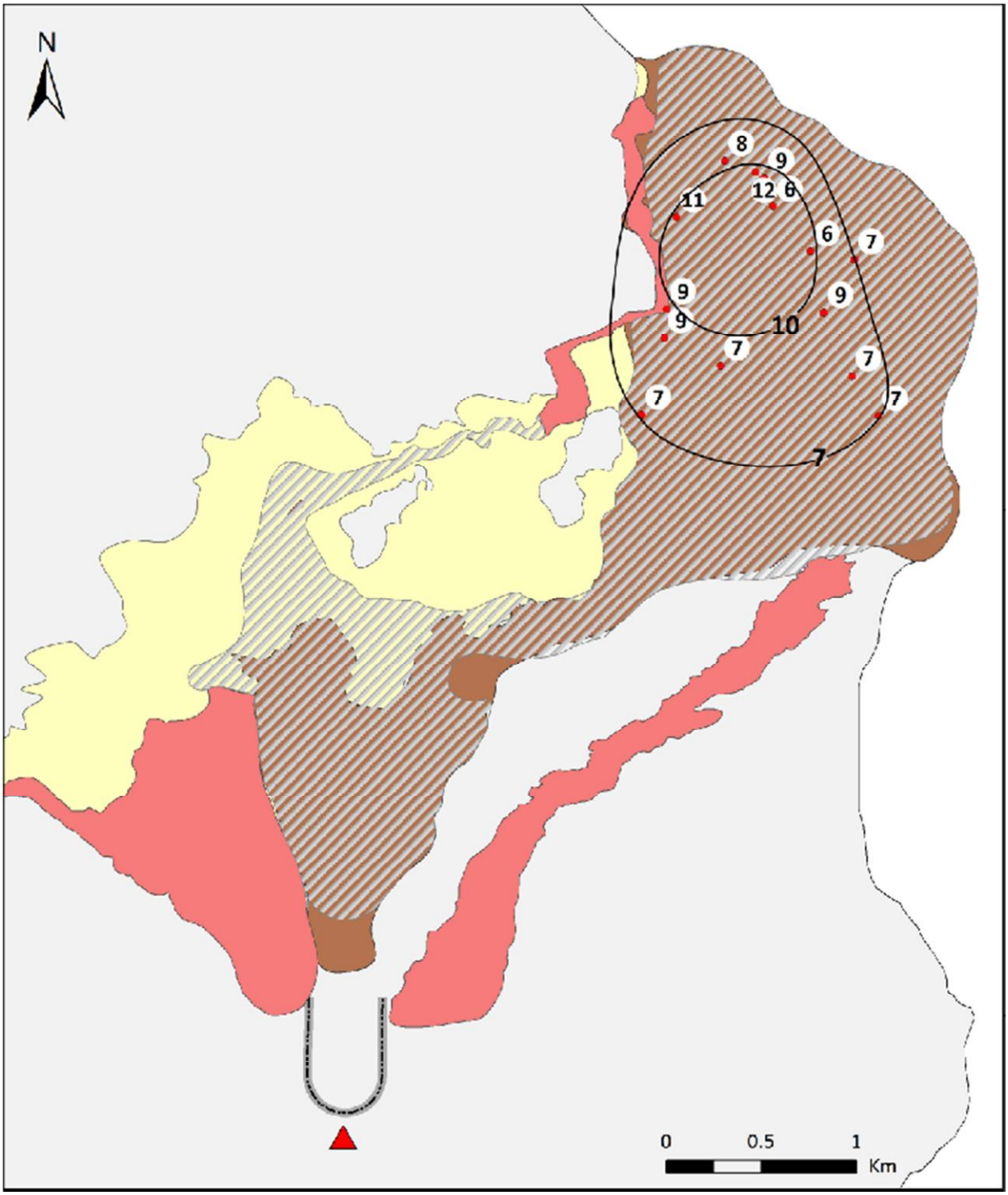

Figure 13: Isopleth map of aggregates (mm) from the co-PDC fallout deposit associated with the 11 February 2010 dome collapse. Legend as in Fig. 1.

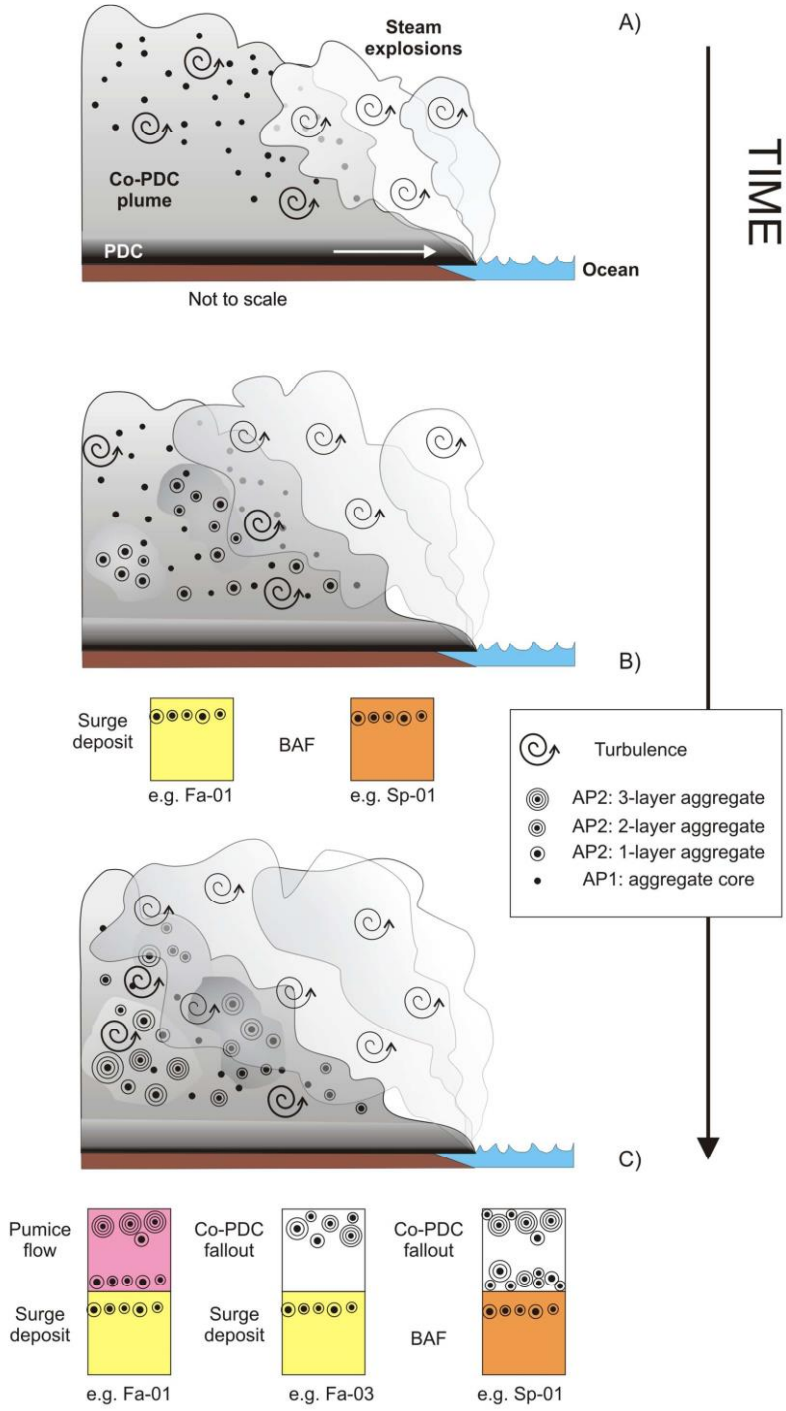

1069

1070 **Figure 14**: Conceptual model for the formation and deposition of particle aggregates during the 11th
1071 February 2010 dome collapse of Soufrière Hills Volcano, Montserrat. Co-PDC plumes generated by
1072 various PDCs (dark grey in Figure) converge into a single cloud (light grey in Figure) and interact with
1073 the vapour clouds generated by the explosions due to the entrance of the PDCs in the sea. Both clouds
1074 are turbulent and enhance both mixing and particle collision. In addition, the vapour clouds provide
1075 additional source of liquid water that enhances particle aggregation. The variety of particle aggregates
1076 (AP1 and both single- and multiple- layer AP2) can be related to the heterogeneity of the co-PDC cloud
1077 (i.e. grainsize and humidity) and to the time evolution of aggregate formation and sedimentation.

1078 Examples of resulting stratigraphy is also shown and compared to Appendix I.

1079